Adverse neurological effects after exposure to copper, manganese and mercury mixtures in a Spraque-Dawley rat model: An ultrastructural investigation

[1]Draper Maxine, [1]Bester Megan Jean, [2]Van Rooy Mia-Jeanne, [1]Oberholzer Hester Magdalena

[1]Department of Anatomy, Faculty of Health Sciences, University of Pretoria, Private Bag x323, Arcadia, 0007, South Africa. [maxinejvr@gmail.com; megan.bester@up.ac.za]

[2]Department of Physiology, Faculty of Health Sciences, University of Pretoria, Private Bag x323, Arcadia, 0007, South Africa. [mia.vanrooy@up.ac.za]

*** Address correspondence to:** H.M. Oberholzer, Department of Anatomy, Faculty of Health Sciences, University of Pretoria Private Bag x323, Arcadia 0007, South Africa. Phone: 0123192533, E-mail: nanette.oberholzer@up.ac.za.

Acknowledgements

The authors would like to thank the National Research Foundation for funding and the staff at the UPBRC for their involvement with the implementation and termination of the animal study and the staff of the Laboratory for Microscopy and Microanalysis of the University of Pretoria, for the use of their microscopes and facilities.

Conflicts of Interest

The author(s) declared no potential conflicts of interest with respect to the research, authorship, and/or publication of this article.

Funding

The author(s) disclosed receipt of the following financial support for the research, authorship, and/or publication of this article: This work was supported by the National Research Foundation under grant number 92768.

Data availability statement

The data that support the findings of this study are available on request from the corresponding author. The data are not publicly available due to privacy or ethical restrictions.

Abstract

Exposure to environmental metal pollutants is linked to oxidative stress and the subsequent development of neurological disease. In this study the effects of copper, manganese and mercury, were evaluated at X100 the World Health Organisation safety limits for drinking water. Using a Sprague-Dawley rat model, following exposure for 28 days, the effects of these metals on biochemical blood parameters and tissue and cellular structure of the brain were determined. Biochemical analysis revealed no hepatocellular injury with minor changes associated with the hepatobiliary system. Minimal changes were found for renal function and the Na^+/K^+ ratio was reduced in the copper and manganese (Cu + Mn) and copper, manganese and mercury (Cu, Mn + Hg) groups that could affect neurological function. Light microscopy of the brain revealed abnormal histopathology of Purkinje cells in the cerebellum and pyramidal cells in the cerebrum as well as tissue damage and fibrosis of the surface blood vessels. Transmission electron microscopy of the cerebral neurons showed microscopic signs of axonal damage, chromatin condensation, the presence of indistinct nucleoli and mitochondrial damage. Together these cellular features suggest the presence and influence of oxidative stress. Exposure to these metals at X100 the safety limits, as part of mixtures, induces changes to neurological tissue that could adversely influence neurological functioning in the central nervous system.

Keywords: copper, manganese, mercury, mixtures, nervous tissue, brain, oxidative stress, cerebellum, cortex.

Introduction

The nervous system is comprised of the central nervous system (CNS) – brain and spinal cord – and the peripheral nervous system. The basic cell components of the CNS are the neurons and glial cells (support cells)[1]. Glial cells include astrocytes, microglia and oligodendrocytes and their precursors with each having their own function in the brain. The microglial cells are the immunological cells of the brain, which are constantly analyzing their environment and reacting to stressors of the brain. They have many similar cellular markers as macrophages [2]. Astrocytes are of high abundance and have many functions in the brain, but the most important are the maintenance of water and ion homeostasis and contributing to and maintaining the blood-brain barrier (BBB) [2]. Mature oligodendrocytes produce myelin for the insulation of

neuronal axons, which allows for rapid signal conduction [2]. Table 1 demonstrates the normal and pathophysiology of various neuronal cells.

Table 1: The physiology and pathophysiology of different neuronal cells present in the brain.

Cell type	Physiology	Pathophysiology
Neurons	Vary greatly in size and shape, and are broadly categorized into large and small neurons. Large neurons are characterized by a large cell body containing a nucleus with single nucleoli and Nissl substance, representing rough endoplasmic reticulum. Most neurons have a single axon, which may branch, and multiple dendrites arising from the cell body [3].	Dark or hyperchromic neurons, degenerating (eosinophilic) neurons and vacuolated neurons. Degenerating neurons are characterized by cell body shrinkage, eosinophilic staining cytoplasm, loss of Nissl substance and a pyknotic, dark staining nucleus that may fragment [3].
Astrocytes	Found between neurons and blood vessels. Astrocytes in grey matter have several stem branches that give rise to many branching processes. Astrocytes in white matter have many long fibre-like processes [4].	Vacuolation and reactive astrogliosis – astrocytes demonstrate a more distinct cytoplasm and larger and eccentric nuclei that may be bi- nucleated and may form a glial scar [3,4].
Oligodendrocytes	Small, round and have a halo or surrounding clear zone [3].	Vacuolation and oedema [3].
Microglia	The smallest glial cells, have a cigar shaped nucleus and are macrophage- like [3,5].	Vacuolation, rod-shaped nuclei and the microglia are generally in close proximity to degenerating neurons and may transform into macrophages and demonstrate a denser infiltration [6].

Physiologically, tissue homeostasis occurs within the brain with the neurons, microglia and astrocytes interacting with each other. In aged brains, an acute pathological state of the brain known as inflammageing occurs, which results in functional impairment due to cellular senescence and the release of pro-inflammatory cytokines by microglia[7]. Chronic neuroinflammation causes an exacerbation of protein aggregate accumulation, neurodegeneration and the release of pro-inflammatory cytokines and chemokines[7]. A decrease in phagocytosis or clearance of damaged neurons is also demonstrated. These features are also demonstrated in pathological states of neurodegeneration [7]. Neurodegeneration is characterised

by progressive neuron dysfunction and death that is associated with oxidative damage and neuroinflammation [8].

The brain is highly susceptible to oxidative stress due to the rich polyunsaturated fatty acid structure of its' neuronal membranes. Oxidative stress can lead to lipid peroxidation of neurons, leading to neuronal necrosis and apoptosis[9]. Oxidative stress is also linked to the development of neurological diseases (ND) such as Parkinson's disease, Alzheimer's disease and amyotrophic lateral sclerosis (ALS) [9,10]. Genetics have a known role in ND's, but it is hypothesized that environmental factors interacting with genes is a probable cause in most individuals [11]. Exposure to environmental pollution, and thus exogenous sources of oxidative stress, is a contributing factor to ND's [9]. Exposure to heavy metals occurs either directly in an occupational setting or indirectly due to the accumulation of metals through exposure in drinking water, food crops, domestic animals and fish[12]. The increased use of heavy metals in industrial-, agricultural-, domestic-, medical-, and technological applications has increased the demand and subsequent release from associated anthropogenic activity, which is a major source of pollution[13, 14].

The neurological effects of several heavy metals have been established. Copper (Cu) and manganese (Mn) are essential micro-nutrients needed for adequate functioning of various biochemical- and physiological processes e.g. cellular respiration, chemical detoxification and metabolism[14,15] Under normal physiological conditions, the BBB is impermeable to these metals and uptake is dependent on specific transporters[16]. If the integrity of the BBB is compromised, these metals can enter the brain, accumulate in the tissue and adversely affect the functioning of the nervous tissue. Majority of Cu is distributed to the liver and a minority to the brain [17]. Copper enters the cerebrospinal fluid (CSF) and in Wilson's disease accumulates in different regions of the brain including the hippocampus, cerebellum, hypothalamus and the cortex[18]. Copper is also known to play a role in NDs such as Parkinson's and Alzheimer's disease. In the disease, the amyloid precursor protein gene molecule contains a Cu-binding site. The binding of Cu^{2+} to amyloid precursor proteins results in the formation of cysteine and two electrons from the oxidation of two cysteine molecules. The one electron reduces Cu^{2+} and the other electron can form •OH. The development of NDs may also be a result of Cu interacting with homocysteine, a thiol-containing amino acid. Homocysteine generates H_2O_2 in the presence of Cu^{2+} and promotes amyloid β protein Cu-mediated H_2O_2 production and neurotoxicity [19].

The brain is one of the main sites of accumulation for Mn. However, it is detectable in CSF before it is detectable in the brain parenchyma [20]. Manganese poisoning or chronic exposure to Mn is associated with Manganism and symptoms include headache, insomnia, memory loss, emotional instability, exaggerated tendon reflexes, hand tremours, speech disturbances and a Parkinsonian gait [21]. Manganese in excess accumulates in the basal ganglia, frontal cortex and cerebellum[18]. In nervous tissue, excess Cu or Mn alters the functionality and structural integrity of proteins, enzymes and receptors resulting in an oxidative stress mediated increase in alpha ($\boldsymbol{\alpha}$)-synuclein aggregation, fibril formation, microglial cell-mediated inflammation and reduced metalloprotein production[18]. Manganese also shifts the ferrous iron ($Fe^{2+)/}$ferric iron ($Fe^{3+)}$ ratio by increasing Fe^{2+} in the brain, which exacerbates oxidative stress and lipid peroxidation [22]. Compared to the mitochondria of other tissues, the mitochondria of the brain are highly sensitive to Cu and possibly other heavy metals as well[23], leading to reactive oxygen species (ROS)-mediated apoptosis and contributing to nervous tissue degeneration.

The neurotoxic effect of mercury (Hg) has been extensively reviewed by Yang *et al.,* 2020[24]. The adverse effects of Hg on neurological development and functioning with both environmental exposure and animal studies, indicated that the developing foetus is the most vulnerable to these effects[25]. The brain and CNS are the main tissue sites for accumulation of elemental Hg [26]. Exposure to elemental and organic Hg via different sources and subsequent pathways of metabolism is associated with neurotoxicity. Mercury accumulates in the glial cells inducing oxidative stress and neuroinflammation[27]. This is because of Hg binding to thiol groups thus adversely affecting glutathione (GSH), a ribosomal protein with microtubule and membrane transport functioning that plays a role as an antioxidant[27]. Astrocytes can produce large amounts of GSH and depletion due to Hg binding adversely affects the role of astrocytes in neurogenesis, synaptogenesis, BBB integrity, extracellular haemostasis and protection against oxidative damage[27]. The binding of Hg to the cysteine residues of tubulin adversely affects the role of microtubules in axonal and dendritic functioning in neuronal tissue. Binding to transporters, such as the glutamate/amino acid transporter (ASCT2), limits amino acid uptake, thereby limiting intracellular GSH synthesis, further contributing to oxidative stress[27]. The increases in ROS, activates inflammatory pathways and in neurological tissue is associated with an increase in microglial cells and associated mediators of inflammation as the microglial cells serve as the first line of defence against foreign invaders[27].

Previously, Africa was considered a low-risk country for heavy metal pollution[28], but with increasing urbanisation, population growth, poor waste management and pollution regulations, extensive environmental contamination has occurred[28]. In Southern Africa, mining together with industrial-, agricultural- and domestic waste contribute to water contamination[28]. Heavy metals in water are generally found as mixtures of two or more metals and are often associated with other compounds, at varying concentrations[29]. Little is known regarding the effects of exposure to metal mixtures containing Cu, Mn and Hg, which are common water contaminants that communities in Southern Africa are commonly exposed. Kenston *et al.,* 2018[30] have studied the systemic toxicity of a metal mixture containing lead (Pb), cadmium (Cd), Hg, Cu, zinc (Zn), Mn, Chromium (Cr) and nickel (Ni) in Sprague-Dawley (SD) rats. Besides systemic toxicity, exposure was associated with reduced cognitive functioning and memory loss[30]. Neurological functioning was also affected in SD pups exposed to Pb, Cd and Hg in drinking water[31]. Although the effects of mixtures on neurological functioning has been postulated according to systemic toxicity[29-32], the effects on the histology of brain tissue in rats have not been determined[32].

In this study the effects of heavy metals as part of mixtures were evaluated based on the limits in water established by the World Health Organisation (WHO) [33]. Using this approach the aim of this study was to investigate the neurological effects on the cerebellum and cerebral cortex of exposure to Cu, Mn and Hg alone and as part of mixtures at concentrations X100 the WHO safety limits in drinking water.

Materials and Methods

Metal preparation

This study used male SD rats exposed to either saline only (control) or to Cu, Mn and Hg, alone and in mixtures. Administration of the aqueous solutions of copper (II) sulphate ($CuSO_4.5H_2O$, purity: 98%), manganese (II) chloride ($MnCl_2.4H_2O$, purity: 99%), mercuric chloride powder ($HgCl_2$, purity: 99%) and 0.9% sodium chloride (NaCl, purity: 99%), which were dissolved in distilled, deionised water (ddH_20), administered via oral gavage. All metal salts were purchased from Sigma-Aldrich, Johannesburg, South Africa. All other reagents were obtained from Sigma Aldrich, Johannesburg, South Africa unless otherwise specified.

Dosage calculations

The final concentration of the daily dosage solutions for each metal and the mixtures are presented in Table 2. The selected concentrations were based on and were X100 greater than the 2011 World Health Organisation's (WHO) drinking water guideline values, for each respective metal (WHO, 2011) [33]. The dosage concentration was chosen based on previous studies that demonstrated moderate adverse effects at the X100 and X1000 WHO concentrations on various systems, including the cardiovascular system (heart and aorta), respiratory system and blood components, exposed to different heavy metal combinations[34-37].

The calculated concentrations were based on a 60 kg adult drinking 2 L of water a day. A 150 g rat equivalent dosage was then calculated, using the following equation:

Rat equivalent dose (mg/kg) = Human equivalent dose (mg/kg) / dosage factor*

*Dosage factor being rat Km/human Km, with the human Km = 37 and the rat Km = 6. The dosage factor for conversion from rat to human is 6/37. Km is a correction factor used based off the surface area of a species[38]. Therefore, the rat equivalent dose was 161.5, 29.6 and 0.17 mg/kg/day for Cu, Mn and Hg, respectively.

Sprague-Dawley rat model

Six-week-old male SD rats (150 g) were obtained from the Onderstepoort Veterinary Animal Research Unit (OVARU). Standard irradiated "Epol" rat pellets and municipal water were provided *ad libitum.* The animals were housed in conventional cages complying with the sizes described in the South African National Standards (SANS) 10386:2008 recommendations. A room temperature of 22°C (±2°C); relative humidity of 50% (±20%) and a 12-hour light/dark cycle was maintained during the entire study. The rats were housed in pairs in cages with autoclaved pinewood shavings as bedding material. White facial tissue paper was added for enrichment according to standard procedures at the University of Pretoria Biomedical Research Centre (UPBRC). The rats were acclimatized for 7 days prior to the start of the 28-day experimentation period. Ethical approval was obtained from the University of Pretoria's Animal Ethics Committee (AEC) with approval number 6/2019.

Forty-eight male rats were included and were randomly divided into eight groups (six rats per group), as follows: control, Cu, Mn, Hg, Cu + Mn, Cu + Hg, Mn + Hg and Cu, Mn + Hg (The control group received a saline solution, 0.9% NaCl, only). The seven experimental groups

received the metal mixtures assigned, at a X100 the WHO safety limit for drinking water (2mg/L for Cu, 0.4mg/L for Mn and 0.06 mg/L for Hg) (WHO, 2011). A rat equivalent dosage was then calculated[22]. All rats were administered 0.5 mL of the respective solutions daily through oral gavage, for 28 days. The rats were weighed bi-weekly to identify any sudden change in weight and the behaviour of the rats was monitored daily. The rats were terminated on day 28 via isoflurane (general anaesthesia) overdose and cardiac puncture, according to the standard methods employed by the UPBRC. Organs were harvested on the day of termination after blood collection via dissection. Neurological tissue was harvested for morphological and ultrastructural analyses.

Organ harvesting and sample preparation

The brains of the animals were harvested on the day of termination via dissection and prepared for light- and transmission electron microscopy according to standard laboratory protocols as described previously by Arbi *et al*., 2021[37].

Blood collection and biochemical parameter testing

Blood was collected on the day of termination via cardiac puncture into a 4.5 mL EVAC EDTA tube. Biochemical and toxicological analyses was performed by the Onderstepoort Clinical Pathology Department. Testing was performed to ascertain the toxicity of the metals in the liver and kidneys, that may contributing to altered neurological functioning.

Light microscopy sample preparation

Following termination, the tissues were dissected from each animal and processed for light microscopy as described by Naidoo *et al*., 2019[35]. The tissue samples were fixed in 4% formaldehyde (FA) in 0.1 M phosphate buffer solution (PBS) [0.2 M disodium phosphate (Na_2HPO_4), 0.2 M sodium dihydrogen phosphate monohydrate ($NaH_2PO_4 \cdot H_2O$), 0.15 M sodium chloride (NaCl), pH: 7.4]. The samples were then washed three times for 30 minutes with 0.1 M PBS, before dehydration using increasing serial concentrations of 50% ethanol (EtOH) (Merck, Johannesburg, South Africa) for 30 minutes, 70% EtOH for one hour, 90% EtOH for one hour, twice in 100% EtOH for one hour and left overnight in 100% EtOH. The samples were infiltrated with paraffin wax by first placing the samples in a 1:1 xylene and

EtOH mixture for 30 minutes, then 100% xylene for 2 hours, followed by 3:7 wax in xylene mixture for one hour, 7:3 wax in xylene mixture for one hour and finally in 100% wax for two hours, all steps at 60°C. The samples were embedded in paraffin wax, cooled to 4°C and then sections of 5 µm were prepared with a Leica RM 2255 wax microtome (Leica Microsystems, Wetzlar, Germany) and placed on glass slides. The sections were de-waxed by placing the slides twice in 100% xylene for five minutes, and then twice in 100% EtOH for two minutes followed by rehydration in 90% and 70% EtOH for one minute each and finally in ddH_2O for 1 minute[35]. The slides were then stained with Haematoxylin and Eosin (H&E) and Picrosirius red (PR) to evaluate general morphology and collagen distribution (fibrosis), respectively.

Haematoxylin and eosin staining

Histopathological analysis was done using images obtained following H&E staining. A 0.1% haematoxylin stain solution was prepared by dissolving 1 g of haematoxylin in 1 L of ddH_2O. To this 0.2 g of sodium iodate and 50 g of potassium aluminium sulphate was then added and dissolved before adding 1 g citric acid and 50 g chloral hydrate. To prepare the eosin stain, 2 g of yellowish eosin powder was dissolved in 200 mL of ddH_2O. Scott's buffer solution was made by dissolving 2 g of potassium bicarbonate and 20 g of magnesium sulphate in 1 L ddH_2O. The sectioned slides were cleared with xylene for 10 min and were rehydrated in a series of decreasing concentrations of EtOH; two changes of 100% EtOH, 90% and 70% each for 1 min. The slides were then placed in ddH_2O for 1 min, haematoxylin for 15 min and Scott's buffer for 8 min. The slides were then rinsed with ddH_2O and then dipped in eosin to counterstain, ascending series of EtOH for rehydration (70% EtOH, 90% EtOH, 100% EtOH) and xylene before the coverslips were mounted with Entellan® mounting medium. The slides were viewed with a Zeiss AXIO Imager.M2 (Zeiss, Oberkochen, Germany) light microscope.

Picrosirius red staining

The PR staining and polarisation method was used to evaluate the orientation of collagen fibres in different tissues under different pathological and physiological states[39]. Collagen appears red, green or yellow under polarized light. A strong yellow-red birefringence indicates collagen type I and a weak greenish birefringence indicates collagen type III[39]. The dye solution was prepared by dissolving 0.5 g of Sirius Red dye in 500 mL of a saturated aqueous solution of picric acid. Acidified water was used for washing, prepared by adding 5 mL of glacial acetic acid to 1 L of ddH_2O. The tissue was first stained in haematoxylin for 8 min and then rinsed

under running tap water for 10 min. The PR solution was applied for 1 hr and the slides were washed twice with acidified water before dehydration three times in 100% EtOH. The slides were cleared with xylene before the coverslip was mounted using Entellan[40]. The slides were viewed with a Zeiss AXIO Imager.M2 (Zeiss, Oberkochen, Germany) light microscope, under brightfield and polarizing light. Representative images of each group were used to evaluate the changes in tissue collagen distribution (fibrosis).

Transmission electron microscopy sample preparation

For ultrastructural studies transmission electron microscopy (TEM) was performed. Samples were obtained from the same area as for light microscopy. The tissue was cut into small pieces of approximately 1 mm^3 in size and then was fixed in a 2.5% glutaraldehyde/formaldehyde (GA/FA) (Sigma-Aldrich, Johannesburg, South Africa) (5 mL 0.075 M PBS – pH 7.4), 1 mL GA, 1 mL FA and 3 mL ddH_2O solution for one hr before being washed three times for 15 minutes in PBS. This was followed by secondary fixation in 1% osmium tetroxide (Sigma-Aldrich, Johannesburg, South Africa) for one hr and washed as described above. The samples were dehydrated by using an increasing serial dehydration step with 30%, 50%, 70% and 90%, followed by three changes of 100% EtOH, 15 minutes for each step. The samples were then left overnight in 100% EtOH and then were finally embedded in resin[37]. The resin blocks were trimmed, and ultra-thin sections (100 nm) were prepared with an ultramicrotome. Samples were contrasted with uranyl acetate for three minutes followed by three minutes of contrasting with lead citrate, after which samples were allowed to air dry before being examined with the JEOL JEM 2100F transmission electron microscope (JEOL Ltd., Tokyo, Japan). Representative images of each group were used to evaluate the changes in tissue ultrastructure.

Statistical analyses

Statistical analysis on the biochemical parameters were performed on GraphPad Prism version 6.01, using one-way analysis of variance (ANOVA) and Tukey's multiple comparisons test. A p-value of ≤ 0.05 was considered significant.

The observational qualitative study of eight animal groups, consisting of the control and seven heavy metal exposed groups, aimed to describe the general structure (H&E staining) and fibrosis (PR staining) in tissue using light microscopy (LM) and the effects on the internal cellular structures using transmission electron microscopy (TEM). The changes in tissue

structure in the exposed groups were compared with the control group. Six rats were included in each group and two slides (LM) or grids (TEM) from each rat were analysed. The sample sizes were adequate as the study was done using a homogenous animal population and had adequate statistical power.

For qualitative comparative purposes an ordinal scoring method was employed by the researcher. The scoring was done according to the severity of histopathological alterations noted by the researcher in the light microscopy analysis and transmission electron microscopy analysis. Scoring was done by direct evaluation of the tissues with values assigned by the observer. The parameters that were evaluated using haematoxylin and eosin staining in the cerebral tissue were the abnormal changes to neurons (Purkinje cells, granule cells and pyramidal cells), infiltration of microglia, and tissue damage/necrosis. The parameters that were evaluated using TEM on the cerebral tissue were the extent of myelin thickening, axonal damage, myelin vacuolation, heterochromatin condensation, indistinction of nucleolus and mitochondrial damage.
For all the parameters the scoring was done as follows:
–: no or minimal alterations; +: slight alteration; ++: moderate alteration and +++: severe alteration.

Results

The results of the biochemical parameters analysed (Table 3), the histopathological findings (Figures 1 – 5), collagen arrangement (Figures 6 and 7) and internal cellular structure (Figures 8 – 10) are described in this section.

Biochemical parameters

Biochemical analysis was performed on the whole blood of the rats and the findings are summarized in Table 3. Important to note is that the brains harvested from the rats did not differ macroscopically with no significant changes to brain mass between the control and experimental groups. Liver function was assessed by measuring different liver enzyme levels and findings are included in Table 3. The concentration of alanine aminotransferase (ALT) and aspartate aminotransferase (AST) showed no statistically significant differences between the groups while alkaline phosphatase (ALP) was significantly reduced when compared with the

control, Cu and Mn vs. Cu, Mn + Hg. Gamma-glutamyl transferase (GGT) was also significantly reduced when compared to the control, activity was reduced for Cu + Mn and the triple combination group (Cu, Mn + Hg). Compared with Cu, GGT concentration was reduced in the Cu + Mn, Cu + Hg and Cu, Mn + Hg groups and compared with Mn was reduced in the Cu + Mn and Cu, Mn + Hg groups. The groups containing Cu had significantly lower concentrations of total bilirubin (T Bil) relative to the control and the Cu only group.

By measuring blood urea nitrogen (BUN) and creatinine (CREA) levels, the effects of the metal exposure on kidney function could also be assessed. Compared with the control, BUN levels were significantly reduced in the Hg and Cu and Mn + Hg groups, while CREA levels were reduced compared to the control for Cu and Hg, and for Cu vs. Cu + Mn and Cu, Mn + Hg. The sodium ion concentration (Na^+) and potassium ion concentration (K^+) were determined as markers of neurological function as these ions play a crucial role in the functioning of the nervous system. The sodium ion concentration did not differ in a statistically significant manner, while the levels of K^+ was significantly increased in groups exposed to Cu, Hg and Mn + Hg. The ratio of sodium ion to potassium ion concentration (Na^+/K^+) was significantly lower for rats exposed to Hg. Between group differences were statistically significant for K^+ for Cu vs. Cu + Mn and for the Na^+/K^+ ratio for Hg vs. Cu, Mn +Hg.

Haemotoxylin and eosin

Histological analysis was performed using H&E staining. Representative images of all the samples included, at X10 and X40 magnification are shown in Figures 1-5. In Figure 1 A1 and A2, cerebellar tissue of the control (saline) group is depicted and demonstrates the cerebellum and its layers: The cerebellar tissue presents with normal structure and arrangement with an outer molecular layer, highly cellular inner granular layer and a Purkinje cell layer located between the molecular and granular layers. The Purkinje cells appear normal (solid black arrow). The cerebellar tissues of the experimental groups are demonstrated in Figures 1 B – D and Figure 2 E – H. In Figures 1 B – D and Figure 2 E – H, with the molecular and granular layers showing normal histology. Some Purkinje cells appear abnormal (hollow black arrows) in all groups (B – H), where the Purkinje cells demonstrated a change in shape (indicated in all except E), an absence of a nucleus and abnormal nucleolar detail (B – H). The experimental

groups (all except C) also demonstrated vacuolation of the tissue (red arrows) although this is most likely due to sample preparation[41].

In Figure 3 A1 and A2, the cerebral cortex of the control (saline) group is depicted together with the layers that the cortex consists of including: the molecular layer (I), the external granular layer (II), the external pyramidal layer (III) and the inner granular layer (IV). The leptomeningeal layer and its associated blood vessels that surround the brain are also indicated (hollow black arrow). The granule and pyramidal neurons as well as the glial cells of the cortex show normal histology. In Figures 3 B – D and 4 E – H, the cerebral cortex of the experimental groups is depicted. The layers of the cortex appear disrupted and show abnormal histology with abnormal pyramidal cells with altered shapes, eosinophillic cytoplasm staining and darkened pyknotic nuclei.

The Cu (Figure 3 B) group demonstrated an increase of pyramidal cells in what should be the external granular layer. The pyramidal cells also demonstrated eosinophillic cytoplasm, loss of nuclear detail and shape changes. The glial cells appeared histologically normal. Intracellular vacuolation (red arrows) was evident in some granule cells and can most likely be attributed to tissue processing. The Mn (Figure 3 C) group also showed uneven distribution of cells in the granular layer (black ring), presumed to be microglia as they can transform into macrophages. The pyramidal cells also demonstrated these pathological features. The granule cells showed no visible morphological alterations. The Hg (Figure 3 D) group also demonstrated uneven cell distribution in the granular layer (black ring) and pathologically abnormal pyramidal cells. The Cu + Mn (Figure 4 E) and Cu + Hg (Figure 4 F) groups both demonstrated abnormal pyramidal cells, with Cu + Mn having the appearance of a thicker molecular layer and Cu + Hg also having increased pyramidal cells in the external granular cell layer as with (B). The Mn + Hg (Figure 4 G) appeared similar to (D) with the uneven distribution of cells in the granular layer (black ring) and abnormal pyramidal cells. The triple mixture group (Figure 4 H) demonstrated pathological pyramidal cells. The leptomeningeal layer and its associated blood vessels that surround the brain are also demonstrated (hollow black arrows), the fibrosis of which will be examined with the PR staining technique.

In Figure 5 A, the larger pyramidal cells of the internal pyramidal layer of the control group are depicted and demonstrates non-pathological large pyramidal cells. The large pyramidal cells of the experimental groups are depicted in Figures 5 B – H and all the groups demonstrate

pathological pyramidal cells at varying degrees demonstrating irregular shape changes, eosinophillic cytoplasm staining and darkened pyknotic nuclei. Some experimental groups also demonstrated tissue damage or necrosis (asterisk) – B, C, E, F, G and H. Vacuolation (red arrows) of the tissue was also evident in all experimental groups (B – H).

A summary on the morphological findings of the brain tissue is presented in Table 4.

Picrosirius Red

Picosirius red was used to assess collagen differentiation and distribution in the leptomeningeal blood vessels surrounding the SD rat brains. Representative images, at X40 magnification, acquired from the stained cerebral cortex, are shown in Figures 6 and 7 under brightfield (1) and polarized light (2). In Figure 6 A2, a representative region of the leptomeningeal blood vessels of the brain of the control (saline) group is depicted and a very dim green birefringence under polarized light is observed. The leptomeningeal blood vessels of the experimental groups are presented in Figures 6 B – D and 7 E – H. An increase in yellow-red birefringence is evident in Cu, Mn, Cu + Mn, Cu + Hg, Mn + Hg and the triple mixture group (Figure 6 B2 and C2 and Figure 7 E2, F2, G2 and H2). The Cu (Figure 6 B2), Mn (Figure 6 C2), Cu +Mn (Figure 7 E2), Mn + Hg (Figure 7 G2) and Cu, Mn + Hg (Figure 7 H2) groups has a slight increase, with Cu + Hg (Figure 7 F2) having a moderate increase in yellow-red birefringence. An increase in yellow-green birefringence was evident in all experimental groups with Cu (Figure 6 B2), Mn (Figure 6 C2), Cu + Mn (Figure 7 E2) and Mn + Hg (Figure 7 G2) having a slight increase, Hg (Figure 6 D2), Cu + Hg (Figure 7 F2) and the triple mixture group (Figure 7 H2) a moderate increase.

Transmission electron microscopy

Representative cerebral micrographs, acquired from control and experimental SD rat brain tissue, are shown in Figures 8-10. In Figures 8A, 9A and 10A, the control (saline) brain tissue no abnormal histopathology was observed. In Figure 8A, neuronal axons (Ax) with myelin sheaths (black arrows) can be observed. Figure 9A demonstrates a neuronal nucleus with central, identifiable nucleolus (n) and mixed hetero- (h) and euchromatin (e). In Figure 10A, mitochondria (m) with regular cristae (white arrows) can be seen. The brain ultrastructure of the experimental groups is demonstrated in Figures 8B - H, 9B - H and 10B - H. The

experimental groups had varying histopathological findings as observed in the nuclei, myelin sheaths and mitochondria. Myelin sheath thickening (blue arrows) and the separation of the layers of the myelin sheath (red arrows) was observed in B and G; axonal damage (green ring) was observed in the Cu + Mn, Cu + Hg and triple mixture groups – Figure 8D, E, F and H. In Figure 9, varying degrees of chromatin condensation (white asterisk) and indistinct nucleoli (n) were demonstrated in all the experimental groups, with the Cu + Mn group (Figure 9E) demonstrating this to the highest degree. In the triple mixture group (Figure 9H), the nucleus presents with an abnormal shape. The loss of mitochondrial (m) integrity (red asterisk) was observed in the Cu + Hg group Cu, Hg, Mn + Hg and the triple mixture group (Figure 10B, D, F, G and H) evident by the loss of the regular arrangement of membrane cristae, whereas Cu + Mn (Figure 10E) demonstrated mitochondrial (m) swelling.

A summary on the ultrastructural findings of the brain tissues is presented in Table 5.

Discussion

Biochemical parameters

The degree of metal toxicity varies between individuals and is based on the dosage of the metal as well as the duration of the exposure. The liver and kidneys are responsible for the removal of heavy metals from the system and are therefore predisposed to damage caused by the accumulation of metals in the body. In order to assess the effect of heavy metal exposure to the functioning of the liver and kidneys, different parameters in the blood of the rats included in this study were analysed to detect any possible functional alterations caused by the heavy metal exposure. Generally, mild to severe liver injury is observed histologically when ALT and AST are double the control mean[42]. The AST and ALT parameters are markers used to assess the integrity and therefore the functioning of hepatic cells. These markers are released into the blood when liver cells are damaged. As the AST and ALT levels of the exposed SD rats did not differ significantly from the control, it can be assumed that liver functioning related to the hepatocytes is normal. The ALP and GGT parameters are markers of hepatobiliary changes, especially when present in high concentrations. The ALP levels were lower for Cu, Mn + Hg as compared with the control and for Cu and Mn compared with the triple metal mixture. However, decreased ALP is not linked to liver dysfunction, but is most likely the result of a build-up of copper in the body as seen with Wilson's disease[43]. The GGT levels were reduced for several combinations compared with the control, as well as single metals compared with the mixtures, also not indicative of liver dysfunction. Measurement of bilirubin assesses the

metabolic function of the liver[42]. The T Bil was compared with the control and was significantly lower for Cu, Mn, Hg and the mixtures Cu + Hg and Cu, Mn + Hg. Low T Bil is not associated with any medical condition, but interesting bilirubin is considered an antioxidant. Consequently in this study, low bilirubin levels may therefore rather indicate the presence of high concentrations of ROS generated upon exposure to heavy metals, rather than liver dysfunction.

The BUN and CREA parameters may be used as markers of compromised kidney function, usually when present in increase concentrations. However, in this study BUN was significantly reduced for rats exposed to Hg and Cu, Mn + Hg as compared with the control. The CREA levels were reduced in Hg compared with the control and Cu vs. Cu + Mn, Cu + Hg and Cu, Mn + Hg, as well as Hg vs. Cu + Hg and the triple metal mixture. A decreased BUN/CREA ratio may be indicative of liver dysfunction, but when assessed together with the ALP, ALT, T Bil and GTT, this is not the case in this study.

The findings of this study are consistent with literature evident in a study by Kenston *et al*., 2018[30] where male SD rats were exposure to a mixture containing, Pb, Cd, Hg, Cu, Zn, Mn, Cr and Ni salts at concentrations of 215, 464 and 1000 mg/kg for 28 days. Kenston *et al*., 2018 found reduced ALP at some concentrations[30]. However, in contrast to this study the T Bil, BUN, CREA, Na^+ and K^+ levels were unchanged. As Na^+ and K^+ are involved in neurological functioning, Kenston et al., 2018 further evaluated neurological functioning using the Morris maze test and found significant neurological changes[30]. In the present study neurological functioning was assessed by studying the microscopic changes present in the brain of the SD rats.

Effects on neurological tissue structure

Chemical homeostasis of the brain is regulated by both the BBB, which separates the blood from the brain interstitial fluid, and the blood-cerebrospinal fluid barrier (BCB), which separates the blood from the cerebrospinal fluid [44]. These barriers protect the brain from many toxicants as both lipid and water-soluble molecules must pass through multiple layers before entering the brain tissue, making these barriers selective for nutrients, drugs and metals, thereby protecting the CNS [44,45]. Endothelial cells of blood vessels surrounding the brain are joined by tight junctions and also contain ATP- dependent transporter proteins, which are resistant to a

multitude of drugs. The capillaries of the brain are also surrounded by astrocytes, which forms a further protective layer [45]. However, all the metals investigated in the present study are able to pass through the BBB. Mercury does this through mimicry; Mn can enter through diffusion, active transport and other mediated transport mechanisms and Cu as free Cu ions via multiple Cu transporters [44,45].

Copper is present throughout the brain, but is highest in the cerebellum, hippocampus and synaptic membranes[46]. Certain studies have demonstrated no or marginal accumulation of Cu in the brain and no changes in neurobehavior[47-49]. However, disturbances in Cu homeostasis have been directly and indirectly associated with neurological and neurodegenerative diseases including Wilson's disease, Alzheimer's disease, Parkinson's disease, and prion disease[50,51]. Impaired Mn homeostasis can also lead to neurodegeneration[52]. Manganese enters the brain through the BBB or blood-cerebrospinal fluid barrier[53]. Excessive Mn accumulation in the brain leads to Manganism that has similar features to Parkinson's disease including motor-, cognitive- and psychiatric abnormalities. Manganism has been reported in workers in the mining, welding and smelting industries exposed to high levels of Mn, as well as communities with drinking water with high concentrations of Mn[52]. Mercury exposure is linked to changes in the CNS and is implicated in several neurological and psychiatric disorders, including Alzheimer's and Parkinson's disease[54,55]. The various species of Hg cause different neuropathologies[55]. In the blood methyl Hg binds to cysteine forming a complex that resembles methionine, but structurally larger. This complex is transported through the BBB into the endothelial cells of the CNS[53]. Mercury is known to induce glial cell reactivity, which is the response of glial cells to CNS injury, an indicator of inflammation in neural tissue[56].

The Purkinje cells in the brain are the sole output neurons of the cerebellar cortex. They integrate information and play a role in the control, coordination and learning of movement[57]. Purkinje cell pathology can be found in both inherited and acquired cerebellar disorders. The degree of pathology is dependent on the cause of cell injury. However, Purkinje cells haveplasticity and thus are resistant to injury and also display a regenerative potential and respond to injury differently compared with other neurons, indicating a compensatory mechanism [58]. Purkinje cells that stain eosinophilic represent Purkinje cells undergoing selective eosinophilic neuronal death. This type of neuronal death can be due to ischaemic damage in the brain and is is different to a focal cerebrovascular event, that damages all cell types in an area, and can take days or weeks to occur dependent on the degree of attack on the

tissue [59]. In a Parkinson's disease rat model, Khadrawy *et al*., 2017 [60] reported changes to Purkinje cells that included pyknotic nuclei, chromatin condensation and a shrunken shape[60].

In the current study, in all the experimental groups (Figure 1 and 2), eosinophillic Purkinje cells with darkened pyknotic nuclei were present, indicating that the metals most likely lead to eosinophilic neuronal death that may cause progressive neurodegeneration of the cerebellum in the long term.

In adult male albino rats, the neurodegenerative effects of Cd included both intra- and extracellular vacuolation, with normal granule cells and pyramidal cells that are irregularly shaped with darkly stained nuclei and pericellular halos[61]. In the current study, all the experimental groups presented with the histologically abnormal pyramidal cells containing eosinophilic cytoplasm and dark-blue stained nuclei consistent with the study by Afifi and Embaby[61] where another heavy metal was studied (Figure 3 and 4). Exposure to gold nanoparticle in albino rats caused distorted pyramidal cells with eosinophillic cytoplasm and darkly stained nuclei within the cerebral cortex[62], corroborating the findings of this study.
Rats exposed to excess Cu (0.15 mg Cu/100 g body weight – lower dosage than current study) using Cu lactate administered by i.p. for 90 days had an increase in swelling and the number of astrocytes as well as degenerating neurons with pyknotic nuclei and dense eosinophilic cytoplasms[63]. Arnal et al. (2013) demonstrated an increase in oxidative biomarkers, anti-oxidant enzyme activity and an increase in the activity of pro-apoptotic markers, calpain and caspase-3 with a Cu overload, especially when administered by i.p [63]. The brain has protective methods against Fe overload, but not against Cu or Mn accumulation and so over-exposure to these metals leads to CNS damage[64].

All the experimental groups showed no or minimal changes to granule cells although the granular layer of the cerebrum appeared to be unevenly distributed. The pyramidal cells of the external pyramidal layer presented with abnormal histology as seen with alterations in shape, darkened and pyknotic nuclei and eosinophillic cytoplasm staining. The Mn, Cu + Mn, Cu + Hg, Mn + Hg and triple mixture (Cu, Mn + Hg) groups (Figure 5 C, E, F, G and H) presented with enlarged pyramidal cells with no clear nuclear definition, possibly representing cellular and extracellular necrosis of the tissues (asterisk). The effects observed strongly indicate that the concentrations of heavy metals included in this study have neurodegenerative effects.

In the current study, the Mn and Mn + Hg groups showed the uneven distribution of cells in the granular layer of the cerebral cortex (Figure 6 and 7 C and G), which was not present in the Cu + Mn and the triple mixture (Cu, Mn + Hg) groups. This suggests that the Mn alters the distribution of cells between the different layers of the cerebral cortex, which is consistent with literature, with Hg being synergistic and Cu being antagonistic when in mixture with Mn. The effects of the heavy metals on neuronal tissue are present in varying degrees in this study where the triple mixture group (Cu, Mn + Hg) demonstrated the most pronounced morphological alterations especially evident in the Purkinje cells, pyramidal cells.

Effects on neuronal cell structure

All three metals included in this study have been associated with neurodegeneration as mentioned previously[65]. Excessive Cu is linked to neurodegenerative disorders through the promotion of synuclein aggregation and the enhancement of amyloid protein aggregation[65]. Furthermore, excessive Cu is also linked to amyotrophic lateral sclerosis due to mutations in Cu/Zn superoxide dismutase leading to an increase in ROS. In prion diseases, excess Cu causes structural changes to prions including high affinity Cu-binding sites that increase resistance against proteosomal degradation[65]. Elevated Mn levels in the brain can cause neurological dysfunction through increasing autophagy, ROS production, mitochondrial dysfunction, transcription of endoplasmic reticulum -related genes and iron dyshomeostasis[65]. Multiple markers of programmed cell death have been found in neurons exposed to Mn[65]. Methyl Hg can cross the BBB and has a high affinity for sulphur groups. Exposure to high levels of methyl Hg can result in high levels of inorganic Hg in the brain. Methyl Hg affects ROS production, neural stem cell differentiation, dopamine metabolism and increases calcium influx, abnormal autophagy, deoxyribose nucleic acid (DNA) damage and mitochondrial dysfunction. It also plays a role in Alzheimer's disease as it increases amyloid proteins in the hippocampus but decreases levels in the cerebrospinal fluid[65]. High levels of Cu and Mn in the brain have been found to activate inflammatory-, oxidative- and nitrosative stress response pathways with increased levels associated with abnormal structural-, regulatory-, and catalytic functions of various proteins, enzymes, receptors and transporters. Neurodegeneration occurs as the metal ions bind to these proteins and subsequently form aggregates, which disrupts mitochondrial function, depletes adenosine tri-phosphate (ATP) and activates apoptosis or necrosis.

In this study, Cu and Mn + Hg were associated with myelin thickening, as well as moderate to severe myelin vacuolation or separation of the layers of the myelin sheath. The latter is the most common pathological feature demonstrated in myelin sheath and is generally thought to be associated with demyelination[66]. During myelination large amounts of ATP are required leading to the production of ROS such as hydrogen peroxide[67]. The build up of ROS together with possible reduced antioxidant activity (as seen with decreased levels of T Bil) may be the reason for the separation of the layers forming the myelin sheath that surrounds the axon. In all the experimental groups, condensed heterochromatin of the nucleus was observed with indistinct nucleoli, predominantly demonstrated in the Cu + Mn and the triple mixture groups. This finding can also be linked to the generation of ROS leading to apoptosis[68.]

Both Hg and Mn are well known for their effects on the neurological system: Methyl mercury is associated with histone modifications, DNA methylation and altered microRNA expression. Unlike the DNA modifications that Mn and Hg cause, Cu accumulation induces changes that affect the cell cycle and apoptosis, through ROS production, DNA damage and p53 activation[68]. The Cu-induced DNA disruption is thought to be due to Cu preferentially binding to certain sites on the DNA strands. The affinity for these sites is even greater than Mn, Cr, Cd, Ni, Zn and magnesium (Mg) [68].

Mitochondrial dysfunction is observed in numerous neurological disorders with dysfunction leading to impaired energy supply, ROS production and apoptosis or necrosis, leading to neurodegeneration. Neurons are dependent on mitochondrial oxidative phosphorylation to meet the high energy demands[69]. Mitochondrial damage was evident in all groups except for the Mn group. Mitochondria appeared enlarged with the loss of cristae integrity as evident in Figure 10. Cristae were evident in Figure 10 E and F, which had enlarged mitochondria. Thus, all experimental groups, except for Mn, demonstrated features of mitochondrial dysfunction indicative of neurodegeneration[69].

Conclusion

In conclusion, the changes to the brain presented in this study demonstrates that the metal ions can cross the BBB and can cause toxic effects, which can predispose an individual to neurological conditions or neurodegenerative disease. This is of concern as in many regions of the world heavy metals in drinking water can be greater than X100 the WHO safety limits. In

addition, changes in common blood biochemical markers poorly reflects the actual impact on neurological tissue. Future studies should focus on the physiological effect of these alterations seen in the neuronal tissue to determine what the effect would be on neurological functioning. Future studies should also focus on quantitative analysis, whereby the thickness of the leptomeninges can be determined to further substantiate the qualitative results. Immunostaining using immunohistochemistry is also a wonderful technique that can be applied to future studies for the confirmation of microglia with CD163 staining and for the confirmation of apoptosis using the terminal deoxynucleotidyltransferase-mediated uridine triphosphate nick-end labelling (TUNEL) assay.

References

1. Kierszenbaum, A.L.; Tres, L. Histology and Cell biology: An Introduction to Pathology. 4th Ed. Elsevier Saunders. 2016.
2. Jäkel, S.; Dimou, L. Glial Cells and Their Function in the Adult Brain: A journey through the history of their ablation. *Front. Cell. Neurosci*. 2017, 11 (24): 1-17.
3. Garman, R.H. Histology of the central nervous system. *Toxicol. Pathol*. 2011, 39(1): 22-35.
4. Sofroniew, M.V.; Vinters, H.V. Astrocytes: biology and pathology. *Acta Neuropathol*. 2010, 119(1): 7-35.
5. Kofler, J.; Wiley, C.A. Microglia: key innate immune cells of the brain. *Toxicol. Pathol.* 2011, 39(1): 103-114.
6. Graeber, M.B.; Streit, W.J. Microglia: biology and pathology. *Acta Neuropathol.* 2010, 119(1):89-105.
7. Scheiblich, H.; Trombly, M.; Ramirez, A.; Heneka, M.T. Neuroimmune connections in ging andneurodegenerative diseases. *Trends Immunol*. 2020, 41(4): 300-312.
8. Dugger, B.N.; Dickson, D.W. Pathology of Neurodegenerative Diseases. *Cold Spring Harb. Perspect. Biol.* 2017, 9(7): 1-47.

9. Singh, A.; Kukreti, R.; Saso, L.; Kukreti, S. Oxidative stress: A key modulator inneurodegenerative diseases. *Molecules*. 2019, 24(8): 1583-1603.
10. Tauffenberger, A.; Magistretti, P.J. Reactive oxygen species: beyond their reactive behavior. *Neurochem. Res.* 2021, 46, 77-87.
11. Cicero, C.E.; Mostile, G.; Vasta, R.; Rapisarda, V.; Signorelli, S.S.; Ferrante, M.; Zappia, M.; Nicoletti, A. Metals and neurodegenerative diseases: A systematic review. *Environ. Res*. 2017, 159: 82-94.
12. Sahu, C., Basti, S. Trace metal pollution in the environment: a review. *Int. J. Environ. Sci. Technol.* 2021, 18, 211–224.
13. El-Demerdash, F.M. Effects of selenium and mercury on the enzymatic activities and lipid peroxidation in brain, liver, and blood of rats. *J. Environ. Sci. Health: B36* 2001, 4, 489-499.
14. Tchounwou, P.B.; Yedjou, C.G.; Patlolla, A.K.; Sutton, D.J. Heavy metals toxicity and the environment. *Exp. Suppl.* 2012, 101 133-164.
15. Wright, R.O.; Baccarelli, A. Metals and neurotoxicology. *J. Nutri.* 2007, 137, 2809-2813.
16. Mezzaroba L, Alfieri DF, Colado Simão AN, Vissoci Reiche EM. 2019. The role of zinc, copper, manganese and iron in neurodegenerative diseases. *Neurotoxicology*, 74: 230-241.
17. Linder, M.C.; Wooten, L.; Cerveza, P.; Cotton, S.; Shulze, R.; Lomeli, N. 1998. Copper transport. *Am. Soc. Clin. Nutr*. 1998, 67(5): 9655-9715.
18. Tarnacka, B.; Jopowicz, A.; Maślińska, M. Copper, iron, and manganese toxicity in neuropsychiatric conditions. *Int. J. Mol. Sci*. 2021, 22, 7820-7849.
19. Gaetke, L.M.; Chow, C.K. Copper toxicity, oxidative stress and antioxidant nutrients. *Toxicology*. 2003, 189: 147-163.

20. O'Neal, S.L.; Lee, J.W.; Zheng, W.; Cannon, J.R. Subacute manganese exposure in rats is aneurochemical model of early manganese toxicity. *Neurotoxicology*. 2014, 44: 303–313.

21. Crossgrove, J.; Zheng, W. Manganese toxicity upon overexposure. *NMR Biomed*. 2004,17(8): 544-553.

22. Chandel, M.; Jain, J.C. Manganese-induced haematological alteration in Wistar rats. *J Environ. Occup. Sci*. 2016, 5(4): 77-81.

23. Borchard, S.; Bork, F.; Rieder, T.; Eberhagen, C.; Popper, B.; Lichtmannegger, J.; Schmitt, S.; Adamski, J.; Klingenspor, M.; Weiss, K-H.; Zischka, H. The exceptional sensitivity of brain mitochondria to copper. *Toxicol. in Vitro*, 2018, 51, 11-22.

24. Yang, L.; Zhang, Y.; Wang, F.; Luo, Z.; Guo, S.; Strähle, U. Toxicity of mercury: molecular evidence. *Chemosphere* 2020, 245, 125586-125700.

25. Caserta, D.; Graziano, A.; Lo Monte, G.; Bordi, G.; Moscarini, M. Heavy metals and placental fetal-maternal barrier: a mini-review on the major concerns. *Eur. Rev. Med. Pharmacol. Sci.* 2013, 17, 2198-2206.

26. Park, J.D. Human exposure and health effects of inorganic and elemental mercury. *J Prev Med Public Health*, 2012, 45: 344-352.

27. Bjørklund, G.; Aaseth, J.; Ajsuvakova, O.P.; Nikonorov, A.A.; Skalny, A.V.; Skalnaya, M.G.; Tinkov, A.A. Molecular interaction between mercury and selenium in neurotoxicity. *Coord. Chem. Rev.* 2017, 332, 30-37.

28. Yabe, J.; Ishizuka, M.; Umemura, T. Current levels of heavy metal pollution in Africa. *J. Vet. Med. Sci.* 2010, 72, 1257-1263.

29. Wildemann, T.M.; Weber, L.P.; Siciliano, S.D. Combined exposure to lead, inorganic mercury and methylmercury shows deviation from additivity for cardiovascular toxicity in rats. *J. Appl. Toxicol.* 2015, 35, 918-926.

30. Kenston, S.S.F.; Su, H.; Li, Z.; Kong, L.; Wang, Y.; Song, X.; Gu, Y.; Barber, T.; Aldinger, J.; Hua, Q.; Li, Z.; Ding, M.; Zhao, J.; Lin, X. The systemic toxicity of heavy metal mixtures in rats. *Toxicol. Res.*2018, 7, 396-407.

31. Zhou, F.; Yin, G.; Gao, Y.; Ouyang, L.; Liu, S.; Jia, Q.; Yu, H.; Zha, Z.; Wang, K.; Xie, J.; Fan, Y.; Shao, L.; Feng, C.; Fan G. Insights into cognitive deficits caused by low-dose toxic heavy metal mixtures and their remediation through a postnatal enriched environment in rats. *J Hazard Mater* 2020, 15, 122081-122117.

32. Su, H.; Li, Z.; Kenston, S.S.F.; Shi, H.; Wang, Y.; Song, X.; Gu, Y.; Barber, T.; Aldinger, J.; Zou, B.; Ding, M.; Zhao, J.; Lin, X. Joint toxicity of different heavy metal mixtures after a short-term oral repeated-administration in rats. *Int. J. Environ. Res. Public Health* 2017, 14, 1164-1182.

33. World Health Organisation: guidelines for drinking-water quality: fourth edition (2011). Available from: https://www.unicef.org/cholera/Chapter_4_prevention/01 _WHO_Guidelines_ for _drinking_water_quality.pdf. Accessed 05 May 2018.

34. Venter C, Oberholzer HM, Cummings FR, Bester MJ. Effects of metals cadmium and chromium alone and in combination on the liver and kidney tissue of male Spraque-Dawley rats: An ultrastructural and electron-energy-loss spectroscopy investigation. *Microscopy Research and Technique*. 2017, 80(8): 878-888.

35. Naidoo SVK, Bester MJ, Arbi S, Venter C, Dhanraj P, Oberholzer HM. 2019. Oral exposure to cadmium and mercury alone and in combination causes damage to the lung

tissue of Spraque-Dawley rats. *Environmental Toxicology and Pharmacology*. 69; 86-94

36. Janse van Rensburg M, van Rooy M, Bester MJ, Serem JC, Venter C, Oberholzer HM. 2019. Oxidative and haemostatic effects of copper, manganese and mercury, alone and in combination at physiologically relevant levels: An *ex vivo* study. *Human and Environmental Toxicology*. 38(4): 419-433
37. Arbi, S.; Bester, M.J.; Pretorius, L.; Oberholzer, H.M. Adverse cardiovascular effects of exposure to cadmium and mercury alone and in combination on the cardiac tissue and aorta of Sprague-Dawley rats. *J. Environ. Sci. Health, Part A* 2021, 56, 609-624.
38. Nair, A.B.; Jacob, S. A simple practice guide for dose conversion between animals and human. *JBCP* 2016, 7, 27-31. Sahu, C.; Basti, S. Trace metal pollution in the environment: a review. *Int. J. Environ. Sci. Technol.* 2021, 18, 211-224.
39. Lattouf R, Younes R, Lutomski D, et al. Picrosirius Red Staining: A Useful Tool to Appraise Collagen Networks in Normal and Pathological Tissues. *Journal of Histochemistry & Cytochemistry*. 2014;62(10):751-758.
40. Velindala, S.; Gaikwad, P.; Ella, K.K.R.; Bhorgonde, K.D.; Hunsingi, P.; Anop, K. Histochemical analysis of polarizing colours of collagen using Picro Sirius red staining in oral submucous fibrosis. *J. Oral Health* 2014, 6, 33-38.
41. Wells GA, Wells M. Neuropil vacuolation in brain: a reproducible histological processing artefact. *J Comp Pathol*. 1989 Nov;101(4):355-62. doi: 10.1016/0021-9975(89)90018-2. PMID: 2691536.
42. Everds, N.E. The role of the toxicological pathologist in informing regulatory decisions and guiding the interpretation and application of data from new technologies and tools. Toxicol. Pathol. 2015, 43, 90-97.

43. Stremmel, W.; Merle, U.; Weiskirchen, R. Clinical features of Wilson disease. *Ann. Trans. Med.* 2019, 7 (Suppl 2), S61. Taber, K.H.; Hurley, R.A. Mercury exposure: effects across the lifespan. C*lin. Neurosci.* 2008, 20, 384-389.

44. Monnot, A.D.; Behl, M.; Ho, S.; Zheng, W. Regulation of brain copper homeostasis by the brain barrier systems: effects of Fe-overload and Fe-deficiency. *Toxicol. Appl. Pharmacol.* 2011, 256(3): 249-257.

45. Charlet, L.; Chapron, Y.; Faller, P.; Kirsch, R.; Stone, A.T.; Baveye, P.C. Neurodegenerative diseases and exposure to the environmental metals Mn, Pb, and Hg. *Coord. Chem. Rev*. 2012, 256, (19–20): 2147-2163.

46. Pal, A.; Badyal, R.K.; Vasishta, R.K.; Attri, S.V.; Thapa, B.R.; Prasad, R. Biochemical, histological, and memory impairment effects of chronic copper toxicity: a model for non-Wilsonian brain copper toxicosis in Wistar rat. *Biol. Trace Elem. Res.* 2013, 153, 257-68.

47. Fujiwara, N.; Iso, H.; Kitanaka, N.; Kitanaka, J.; Eguchi, H.; Ookawara, T.; Ozawa, K.; Shimoda, S.; Yoshihara, D.; Takemura, M.; Suzuki, K. Effects of copper metabolism on neurological functions in Wistar and Wilson's disease model rats. *Biochem. Biophys. Res. Commun.* 2006, 349, 1079-1086.

48. Leiva, J.; Palestini, M.; Infante, C.; Goldschmidt, A.; Motles, E. Copper suppresses hippocampus LTP in the rat, but does not alter learning or memory in the morris water maze. *Brain Res.* 2009,1256, 69-75.

49. Özcelik, D.; Uzun, H. Copper intoxication; antioxidant defenses and oxidative damage in rat brain. *Biol. Trace Elem. Res.* 2009, 127, 45-52.

50. Desai, V.; Kaler, S.G. Role of copper in human neurological disorders. *Am. J. Clin. Nutri.* 2008, 88, 855-858.

51. Monnot, A.D.; Behl, M.; Ho, S.; Zheng, W. Regulation of brain copper homeostasis by the brain barrier systems: effects of Fe-overload and Fe-deficiency. *Toxicol. Appl. Pharmacol.* 2011, 256, 249-257.

52. Dusek, P.; Roos, P.M.; Litwin, T.; Schneider, S.A.; Flaten, T.P.; Aaseth, J. The neurotoxicity of iron, copper and manganese in Parkinson's and Wilson's diseases. *J. Trace Elem. Med. Biol.* 2015, 31:193-203.

53. Charlet, L.; Chapron, Y.; Faller, P.; Kirsch, R.; Stone, A.T.; Baveye, P.C. Neurodegenerative diseases and exposure to the environmental metals Mn, Pb, and Hg. *Coord. Chem. Rev.* 2012, 256, 2147-2163.

54. Xu, F.; Farkas, S.; Kortbeek, S.; Zhang, F.X.; Chen, L.; Zamponi, G.W.; Syed, N.I. Mercury-induced toxicity of rat cortical neurons is mediated through N-Methyl-D-Aspartate receptors. *Mol. Brain* 2012, 5, 30-64.

55. O'Donoghue, J.L.; Watson, G.E.; Brewer, R.; Zareba, G.; Eto, K.; Takahashi, H.; Marumoto, M.; Love, T.; Harrington, D.; Myers, G.J. Neuropathology associated with exposure to different concentrations and species of mercury: A review of autopsy cases and the literature. *Neurotoxicol.* 2020, 78, 88-98.

56. Farina, M.; Avila, D.S.; da Rocha, J.B.; Aschner, M. Metals, oxidative stress and neurodegeneration: a focus on iron, manganese and mercury. *Neurochem. Int.* 2013, 62, 575-594.

57. Glickstein, M.; Doron, K. Cerebellum: connections and functions. *Cerebellum* 2008, 7, 589-594.

58. Kemp, K.C; Cook, A.J.; Redondo, J.; Kurian, K.M.; Scolding, N.J.; Wilkins, A. Purkinje cell injury,structural plasticity and fusion in patients with Friedreich's ataxia. *Acta Neuropathol. Commun*. 2016, 4(1): 53-68.

59. Björklund, E.; Lindberg, E.; Rundgren, M.; Cronberg, T.; Friberg, H.; Englund, E. Ischaemic brain damage after cardiac arrest and induced hypothermia - a systematic description of selective eosinophilic neuronal death: A neuropathologic study of 23 patients. *Resuscitation*. 2014, 85(4): 527- 532.

60. Khadrawy, Y.A.; Salem, A.M.; El-Shamy, K.A.; Ahmed, E.K.; Fadl, N.N.; Hosny, E.N. Neuroprotective and therapeutic effect of caffeine on the rat model of parkinson's disease induced by rotenone. *J. Diet. Suppl.* 2017, 14, 553-572.

61. Afifi, O.K.; Embaby, A.S. Histological Study on the protective role of ascorbic acid on cadmium induced cerebral cortical neurotoxicity in adult male albino rats. *J. Micros. Ultrastruct.* 2016, 4, 36-45.

62. El-Drieny, E.A.E.A.; Sarhan, N.I.; Bayomy, N.A.; Elsherbeni, S.A.E.; Momtaz, R.; Mohamed, H.E. Histological and immunohistochemical study of the effect of gold nanoparticles on the brain of adult male albino rat. *J. Micros. Ultrastruct.* 2015, 3, 181-190.

63. Arnal, N.; Morel, G.R.; de Alaniz, M.J.; Castillo, O.; Marra, C.A. Role of copper and cholesterol association in the neurodegenerative process. *Int J Alzheimers Dis.* 2013, 2013:1-41.

64. Dusek, P.; Roos, P.M.; Litwin, T.; Schneider, S.A.; Flaten, T.P.; Aaseth, J. The neurotoxicity of iron, copper and manganese in Parkinson's and Wilson's diseases. *J Trace Elem Med Biol.* 2015, 31:193-203.

65. Chen, P.; Miah, M.R.; Aschner, M. Metals and neurodegeneration. *F1000Research* 2016, 5, 1-42.

66. Duncan ID, Radcliff AB. Inherited and acquired disorders of myelin: The underlying myelin pathology. *Exp. Neuro.* 2016, 283, 452-475.

67. Bradl, M.; Lassmann, H. Oligodendrocytes: biology and pathology. *Acta Neuropathol.* 2010, 119, 37-53.

68. Tassabehji, N.M.; Van Landingham, J.W.; Levenson, C.W. Copper alters the conformation and transcriptional activity of the tumor suppressor protein p53 in human Hep G2 cells. *Exp. Biol. Med* 2005, 230, 699-708.

69. Zhao, X.Y.; Lu, M.H.; Yuan, D.J.; Xu, D.E.; Yao, P.P.; Ji, W.L.; Chen, H.; Liu, W.L.; Yan, C.X., Xia, Y.Y.; Li, S.; Tao, J.; Ma, Q.H. Mitochondrial Dysfunction in Neural Injury. *Front. Neurosci.* 2019, 13, 30-44.

Tables

Table 2: Daily dosage calculations for the oral gavage solutions of the experimental groups.

	Cu	Mn	Hg
WHO limit (mg/L)	**2.0**	**0.4**	**0.006**
WHO limit X 100 (mg/L)	200.0	40.0	0.6
Molecular weight: metal (g/mol)	63.5	54.9	200.6
Metal ion concentration (mM)	3.147	0.728	0.003
Molecular weight: metal-salt (g/mol)	249.7	197.9	271.5
Metal salt concentration (g/L)	0.786	0.144	0,0008
Daily intake (g/2L)	1.572	0.288	0.0016
Human (60 kg) daily intake (mg/kg)	26.2	4.8	0.027
Rat (150 g) intake (mg/kg)	161.5	29.6	0.17
Dosage solutions (mg/mL)	**48.5**	**8.9**	**0.05**

*Note: Mixtures contain the same (mg) of each respective metal.

Table 3: The mean ± SD of the liver and kidney functions of control and exposed rats.

Control[a]	Cu[b]	Mn[c]	Hg[d]	Cu + Mn	Cu + Hg	Mn + Hg	Cu, Mn + Hg
				ALT (U/L)			
69.6 ± 7.7	69.9 ± 18.7	65.2 ± 6.6	62.2 ± 12.1	172.2 ± 164.7,	80.8 ± 23.7	69.1 ± 1.3	70.3 ± 6.8
				AST (U/L)			
101 ± 20	117 ± 28	97 ± 16	100 ± 28	241 ± 257	122 ± 56	106 ± 9	96 ± 17
				ALP (U/L)			
217 ± 14	213 ± 23	219 ± 18	199 ± 16	213 ± 23	217 ± 17	214 ± 23	189 ± 13 [a, b, c]
				GGT (U/L)			
1.3 ± 1.5	2.2 ± 1.3	1.8 ± 1.7	1.7 ± 1.4	0.0 ± 0.0 [a,b]	0.2 ± 0.4 [b, d]	1.2 ± 0.8	0.0 ± 0.0 [a,b,c]
				T Bil (µmol/L)			
1.5 ± 0.2	1.2 ± 0.2 [a]	1.1 ± 0.4 [a]	1.2 ± 0.3 [a]	1.4 ± 0.3	0.9 ± 0.4 [a, b]	1.1 ± 0.3 [a]	1.0 ± 0.3 [a, b]
				BUN (mmol/L)			
6.9 ± 0.3	6.7 ± 0.6	6.7 ± 0.7	6.6 ± 0.4 [a]	6.7 ± 0.7	6.9 ± 0.5	6.9 ± 0.5	6.4 ± 0.4 [a]
				CREA (µmol/L)			
28.2 ± 0.8	26.0 ± 2.2 [a]	27.5 ± 2.1	23.8 ± 2.9 [a]	29.2 ± 1.2 [b]	28.8 ± 2.6 [b, d]	27.2 ± 2.3	28.7 ± 2.3 [b, d]
				Na^+ (mmol/L)			
142 ± 1.2	142 ± 1.2	142 ± 0.8	141 ± 0.5	142 ± 0.8	142 ± 1.5	141 ± 1.0	142 ± 1.6

				K^+ (mmol/L)			
3.6 ± 0.4	3.9 ± 0.3 [a]	3.7 ± 0.3	4.1 ± 0.3 [a]	3.4 ± 0.3 [b]	3.7 ± 0.3	3.9 ± 0.2 [a]	3.7 ± 0.3 [d]
				Na^+/K^+ratio			
43.9 ± 4.0	36.3 ± 2.6	38.1 ± 3.2	34.8 ± 2.3[a]	40.0 ± 3.4 [b]	38.4 ± 3.3	35.9 ± 2.3	38.5 ± 3.38 [d]

Data is an average ± Standard deviation (*SD).* The following symbols indicate significant differences: a: between the control and each metal and combinations, b: between Cu vs. metal combinations containing Cu, c: Mn vs. metal combinations containing Mn, d: Hg vs. metal combinations containing Hg. ALT = Alanine Aminotransferase, AST = Aspartate Aminotransferase, ALP = Alkaline Phosphatase, GGT = Gamma-glutamyl transferase, T Bil = Total Bilirubin, BUN = Blood urea nitrogen, CREA = Creatinine, Na^+ = Sodium ion, K^+ = Potassium ion.

Table 4: Summary of the histological changes to the H&E stained brain (cerebellum and cortex) following metal exposure.

	Neuronal pathology			Support (glial) cells	Tissue damage/ Necrosis
	Purkinje cells	Granule cells	Pyramidal cells		
Cu	+	+	++	-	+
Mn	+	-	+++	+	+++
Hg	++	-	++	++	-
Cu + Mn	++	-	++	-	+
Cu + Hg	++	-	++	-	+
Mn + Hg	+	-	+++	++	++
Cu, Mn + Hg	+++	+	+++	-	++

–: no or minimal alterations; +: slight alteration; ++: moderate alteration; +++: severe alteration.

Table 5: Summary of the ultrastructural changes to cerebral tissue following metal exposure.

	Myelin		Axon	Intracellular		
	Thickening	Degree of layer separation of myelin sheath	Damage	Chromatin condensation	Indistinct nucleolus	Mitochondrial damage
Cu	+	++	++	+	+	++
Mn	-	-	-	+	+	-
Hg	-	-	++	+	+	++
Cu + Mn	-	-	+	+++	++	++
Cu + Hg	-	-	+++	-	++	++
Mn + Hg	+	+++	-	+	++	++
Cu, Mn + Hg	-	+	+	++	+++	++

–: no or minimal alterations; +: slight alteration; ++: moderate alteration; +++: severe alteration

Figure legends

Figure 1: Micrographs of SD rat brain cerebellum stained with H&E for the control and single heavy metal groups. **A**: Control, **B**: Cu, **C**: Mn, **D**: Hg. **WM**: White matter; **ML**: Molecular layer; **GL**: Granular layer; **P**: Purkinje cells; **Solid black arrow**: Normal Purkinje cell; **Hollow black arrow**: Pathological Purkinje cell; **Red arrow**: Vacuolation and **Black box**: The area of the cerebellum in 1 that is magnified in 2. **1**: X10 magnification: scale bar = 100 µm; **2**: X40 magnification: scale bar = 20 µm.

Figure 2: Micrographs of SD rat brain cerebellum stained with H&E for the double and triple heavy metal mixture groups. **E**: Cu + Mn, **F**: Cu + Hg, **G**: Mn + Hg, and **H**: Cu, Mn + Hg. **WM**: White matter; **ML**: Molecular layer; **GL**: Granular layer; **P**: Purkinje cells; **Solid black arrow**: Normal Purkinje cell; **Hollow black arrow**: Pathological Purkinje cell; **Red arrow**: Vacuolation and **Black box**: The area of the cerebellum in 1 that is magnified in 2. **1**: X10 magnification: scale bar = 100 µm; **2**: X40 magnification: scale bar = 20 µm.

Figure 3: Micrographs of SD rat brain cerebral cortex stained with H&E for the control and single heavy metal groups. **A**: Control, **B**: Cu, **C**: Mn, **D**: Hg. **I**: Molecular layer; **II**: External granular layer; **III**: External pyramidal layer; **IV**: Inner granular layer; **Pyr**: Pyramidal cells; **Gr**: Granule cells; **Gl**: Glial cells; **BV**: Blood vessel; **Hollow black arrow**: Leptomeninges; **Black ring**: Uneven distribution of cells in the granular layer and **Red arrow**: Vacuolation. **1**: X10 magnification: scale bar = 100 µm; **2**: X40 magnification: scale bar = 20 µm.

Figure 4: Micrographs of SD rat brain cerebral cortex stained with H&E for the double and triple heavy metal mixture groups. **E**: Cu + Mn, **F**: Cu + Hg, **G**: Mn + Hg, and **H**: Cu, Mn + Hg. **I**: Molecular layer; **II**: External granular layer; **III**: External pyramidal layer; **IV**: Inner granular layer; **Pyr**: Pyramidal cells; **Gr**: Granule cells; **Gl**: Glial cells; **BV**: Blood vessel; **Hollow black arrow**: Leptomeninges; **Black ring**: Uneven distribution of cells in the granular layer and **Red arrow**: Vacuolation. **1**: X10 magnification: scale bar = 100 µm; **2**: X40 magnification: scale bar = 20 µm.

Figure 5: Micrographs of SD rat brain cerebral cortex stained with H&E demonstrating pyramidal cells of the internal pyramidal layer; Scale bar = 20 µm. **A**: Control, **B**: Cu, **C**: Mn, **D**: Hg, **E**: Cu + Mn, **F**: Cu + Hg, **G**: Mn + Hg, and **H**: Cu, Mn + Hg. **Pyr**: Pyramidal cells; **Asterisk (*)**: Tissue damage/necrosis and **Red arrow**: Vacuolation.

Figure 6: Micrographs of SD rat brain stained with PR for the control and single heavy metal groups depicting the collagen of the leptomeningeal blood vessels surrounding the brain; Scale bar = 20 µm. **A**: Control, **B**: Cu, **C**: Mn, **D**: Hg. **1**: Brightfield and **2**: Polarized light

Figure 7: Micrographs of SD rat brain stained with PR for the double and triple heavy metal mixture groups depicting the collagen of the leptomeningeal blood vessels surrounding the brain ; Scale bar = 20 µm. **E**: Cu + Hg, **F**: Cu + Mn, **G**: Mn + Hg, and **H**: Cu, Mn + Hg. **1**: Brightfield and **2**: Polarized light.

Figure 8: TEM micrographs of cerebral tissue of SD rats exposed to Cu, Mn and Hg metal mixtures showing the ultrastructure of the tissue and demonstrating neuronal axons surrounded by myelin sheath; Scale bar = 2000 nm. **A**: Control, **B**: Cu, **C**: Mn, **D**: Hg, **E**: Cu + Mn, **F**: Cu + Hg, **G**: Mn + Hg, and **H**: Cu, Mn + Hg. **Black Arrows**: Myelin sheath; **Ax**: Axon; **Red arrows**: Separation of layers of myelin; **Green ring**: axonal damage; **Blue arrows**: Myelin thickening and **m**: mitochondria.

Figure 9: TEM micrographs of cerebral tissue of SD rats exposed to Cu, Mn and Hg metal mixtures showing the ultrastructure of the tissue and demonstrating the ultrastructure of the nuclei within neurons; Scale bar = 1000 nm. **A**: Control, **B**: Cu, **C**: Mn, **D**: Hg, **E**: Cu + Mn, **F**: Cu + Hg, **G**: Mn + Hg, and **H**: Cu, Mn + Hg. **n**: nucleolus; **h**: heterochromatin; **e**: euchromatin; **White asterisk**: condensed chromatin.

Figure 10: TEM micrographs of cerebral tissue of SD rats exposed to Cu, Mn and Hg metal mixtures showing the ultrastructure of neuronal mitochondria; Scale bar = 1000 nm. **A**: Control, **B**: Cu, **C**: Mn, **D**: Hg, **E**: Cu + Mn, **F**: Cu + Hg, **G**: Mn + Hg, and **H**: Cu, Mn + Hg. **m**: mitochondria, **White arrows**: cristae and **Red asterisk**: Loss of mitochondrial integrity.

Figure 1

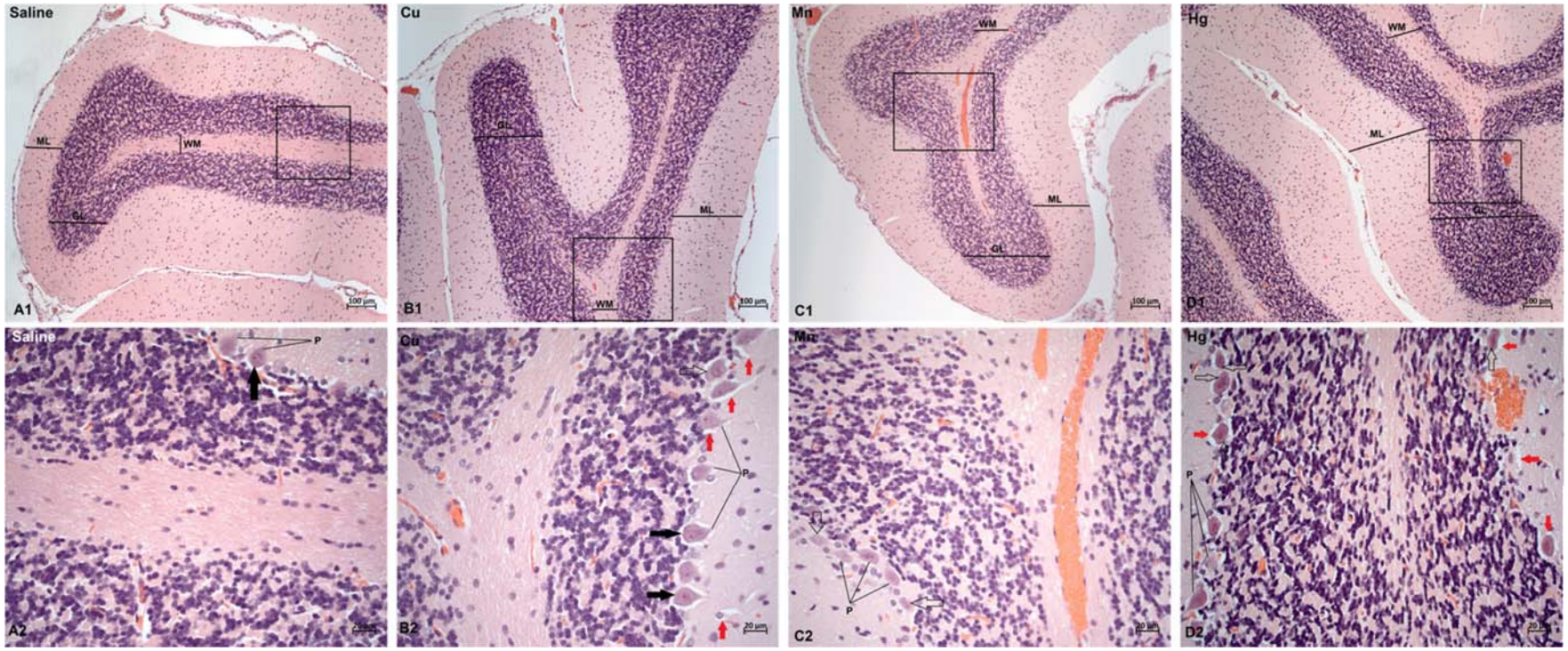
Saline
ML
WM
GL
A1
100 µm
Cu
GL
ML
WM
B1
100 µm
Mn
WM
ML
GL
C1
100 µm
Hg
WM
ML
GL
D1
100 µm
Saline
P
A2
20 µm
Cu
P
B2
20 µm
Mn
P
C2
20 µm
Hg
P
D2
20 µm

Figure 2

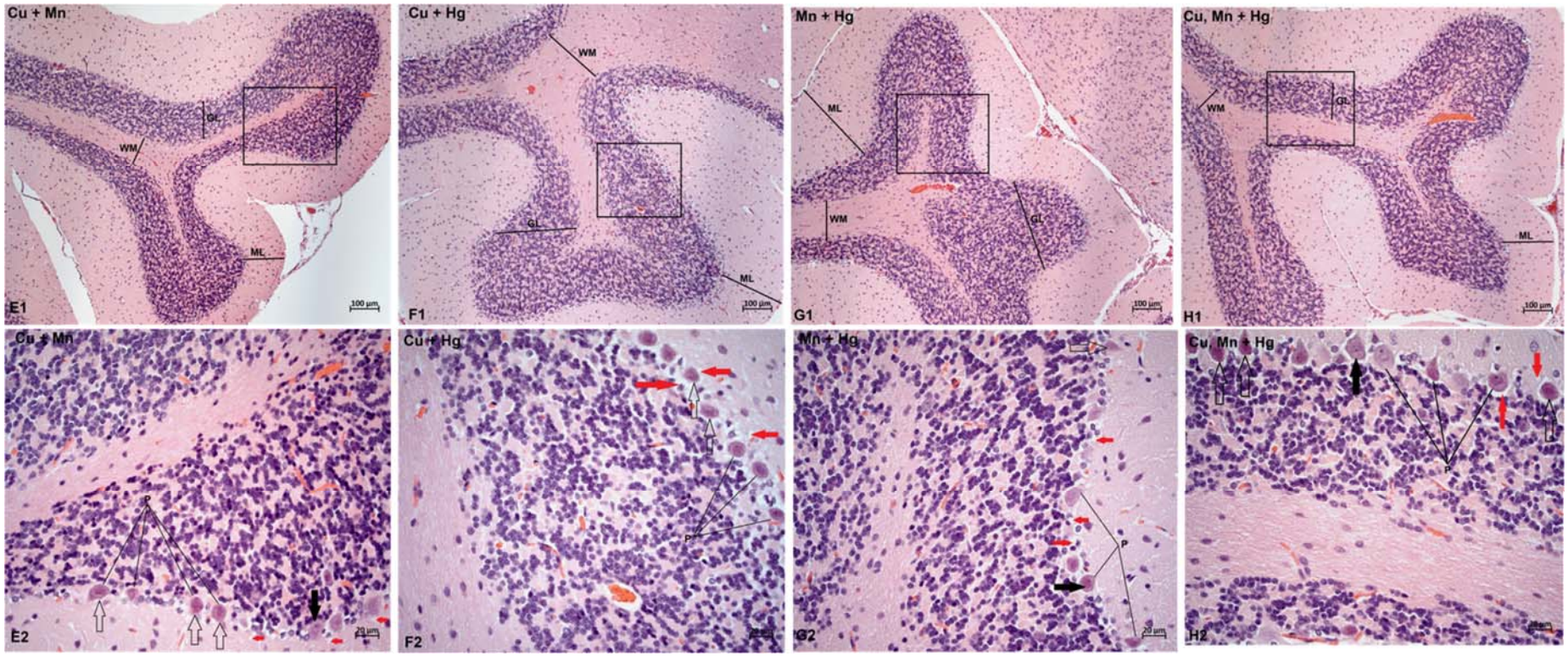
Cu + Mn
GL
WM
ML
E1
100 µm
Cu + Hg
WM
GL
ML
F1
100 µm
Mn + Hg
ML
WM
GL
G1
100 µm
Cu, Mn + Hg
WM
GL
ML
H1
100 µm
Cu + Mn
P
E2
20 µm
Cu + Hg
P
F2
20 µm
Mn + Hg
P
G2
20 µm
Cu, Mn + Hg
P
H2
20 µm

Figure 3

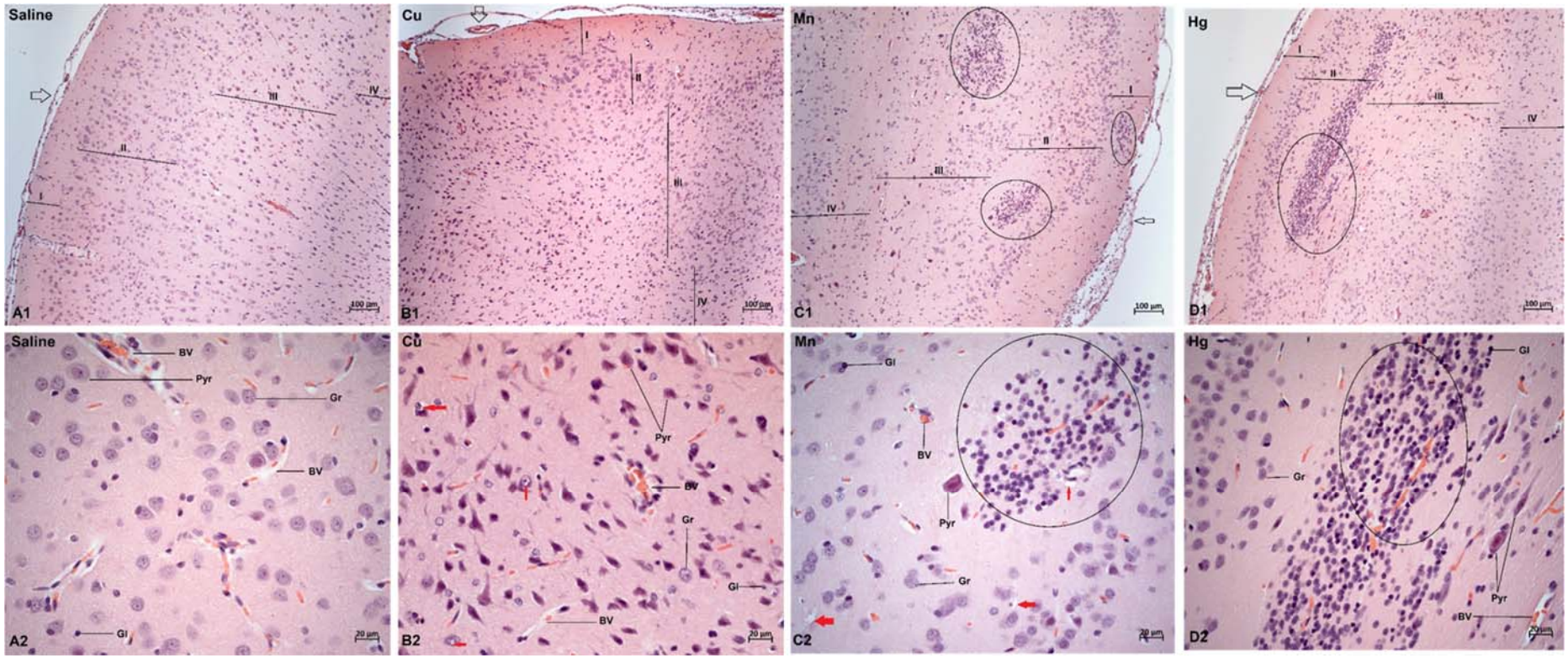
Saline
Cu
Mn
Hg
A1
B1
C1
D1
A2
B2
C2
D2
I
II
III
IV
BV
Pyr
Gr
Gl
100 µm
20 µm

Figure 4

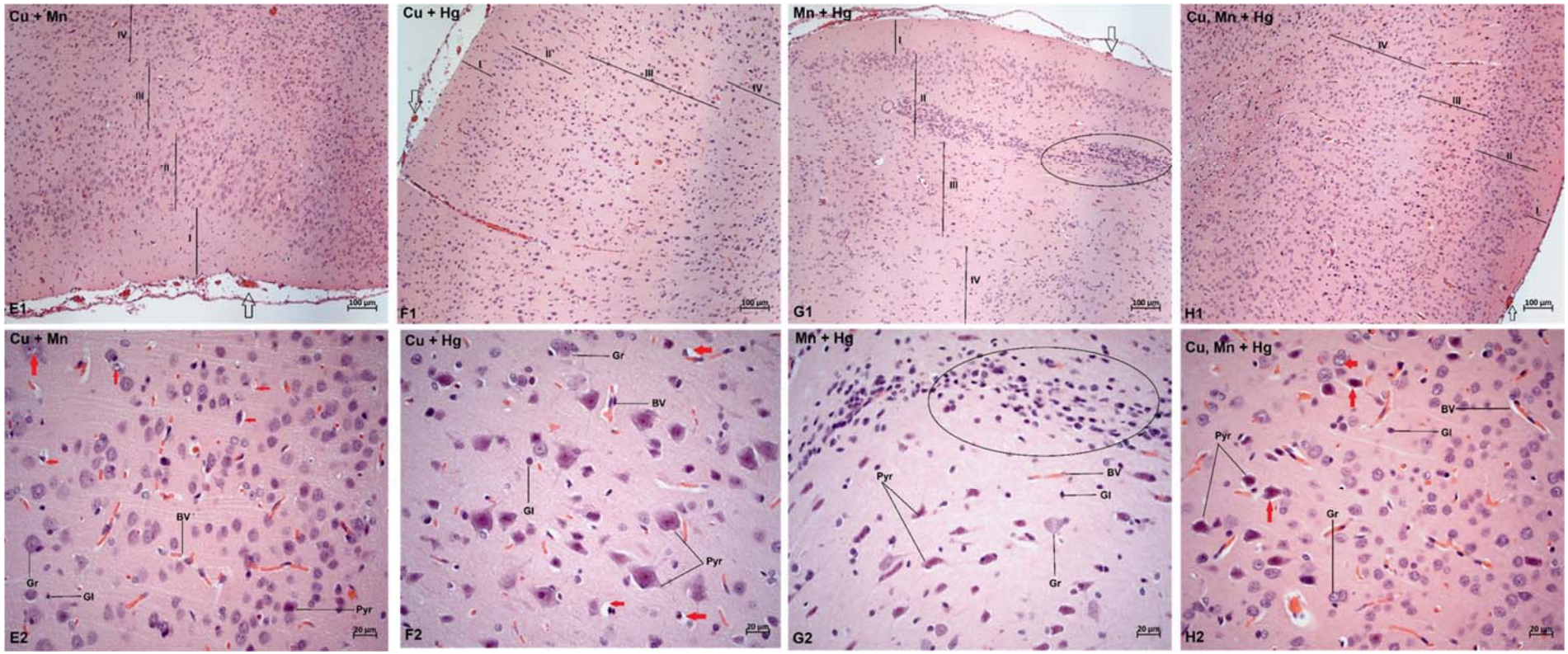
Cu + Mn
IV
III
II
I
E1
100 µm
Cu + Hg
I
II
III
IV
F1
100 µm
Mn + Hg
I
II
III
IV
G1
100 µm
Cu, Mn + Hg
IV
III
II
I
H1
100 µm
Cu + Mn
BV
Gr
Gl
Pyr
E2
20 µm
Cu + Hg
Gr
BV
Gl
Pyr
F2
20 µm
Mn + Hg
Pyr
BV
Gl
Gr
G2
20 µm
Cu, Mn + Hg
BV
Gl
Pyr
Gr
H2
20 µm

Figure 5

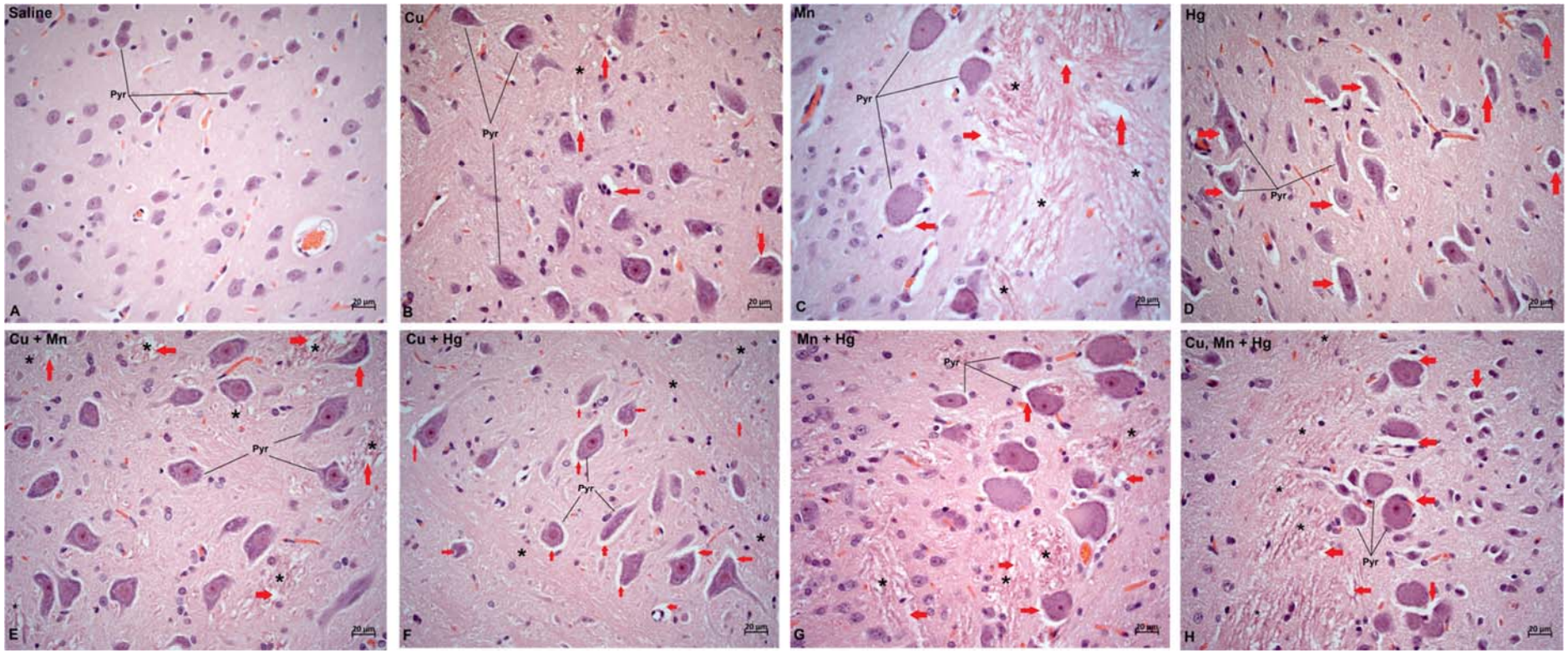
Saline
Pyr
A
20 µm
Cu
Pyr
B
20 µm
Mn
Pyr
C
20 µm
Hg
Pyr
D
20 µm
Cu + Mn
Pyr
E
20 µm
Cu + Hg
Pyr
F
20 µm
Mn + Hg
Pyr
G
20 µm
Cu, Mn + Hg
Pyr
H
20 µm

Figure 6

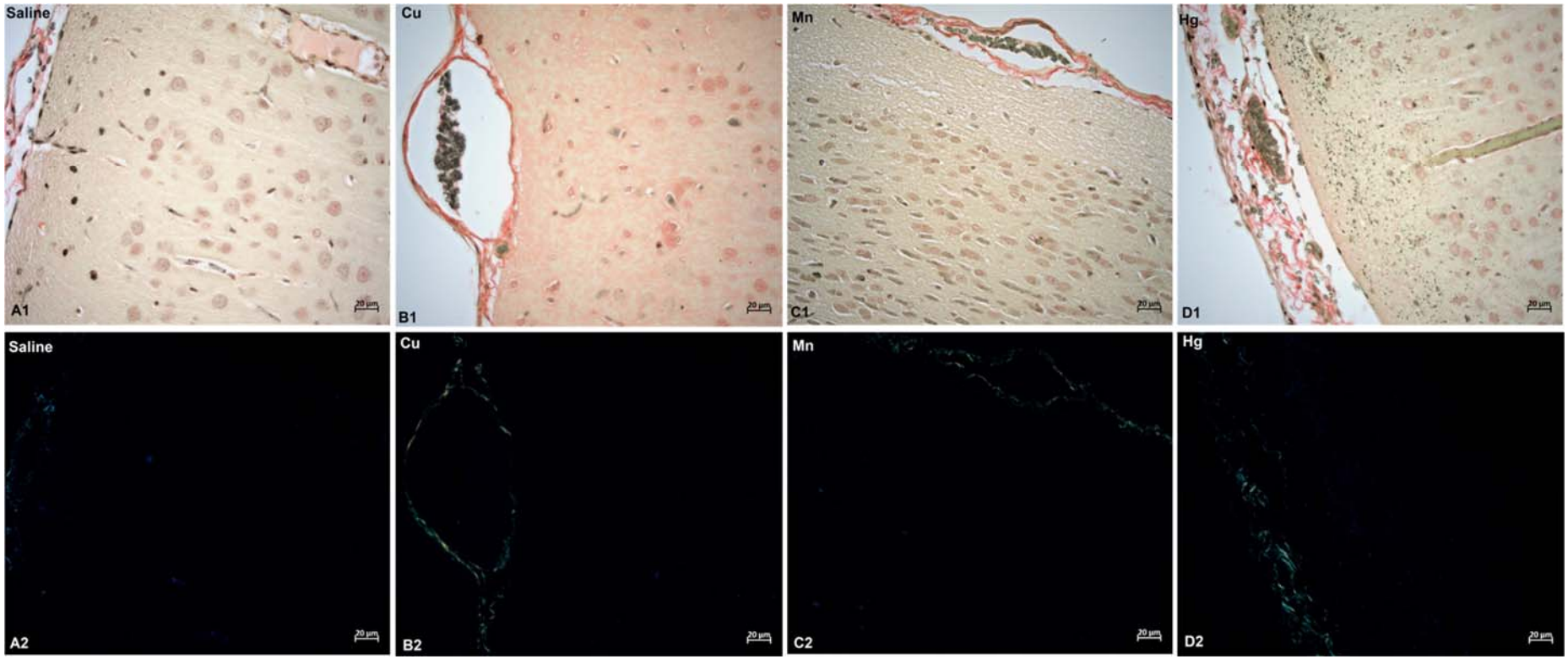

Figure 7

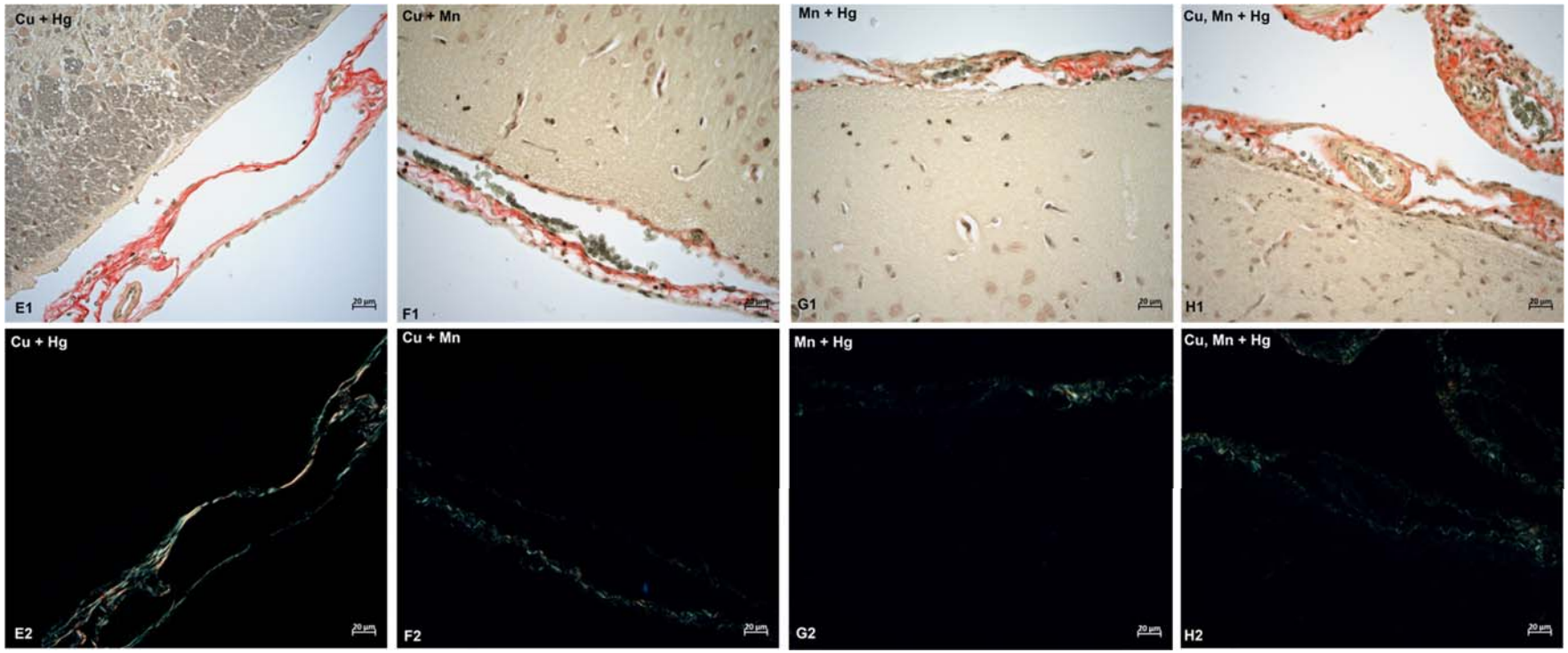
Cu + Hg
E1
Cu + Mn
F1
Mn + Hg
G1
Cu, Mn + Hg
H1
Cu + Hg
E2
Cu + Mn
F2
Mn + Hg
G2
Cu, Mn + Hg
H2

Figure 8

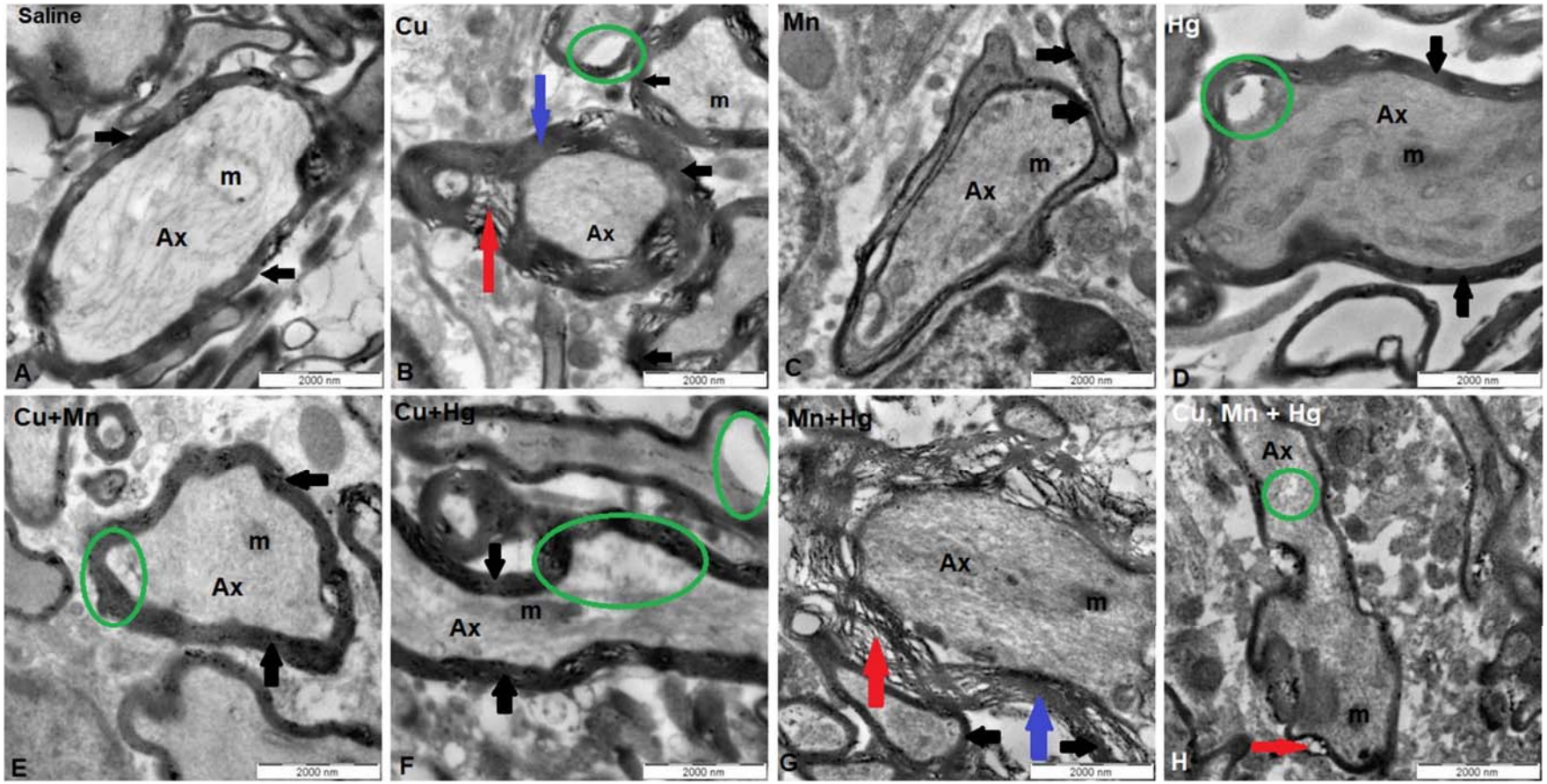
Saline
m
Ax
A
2000 nm
Cu
m
Ax
B
2000 nm
Mn
m
Ax
C
2000 nm
Hg
Ax
m
D
2000 nm
Cu+Mn
m
Ax
E
2000 nm
Cu+Hg
m
Ax
F
2000 nm
Mn+Hg
Ax
m
G
2000 nm
Cu, Mn + Hg
Ax
m
H
2000 nm

Figure 9

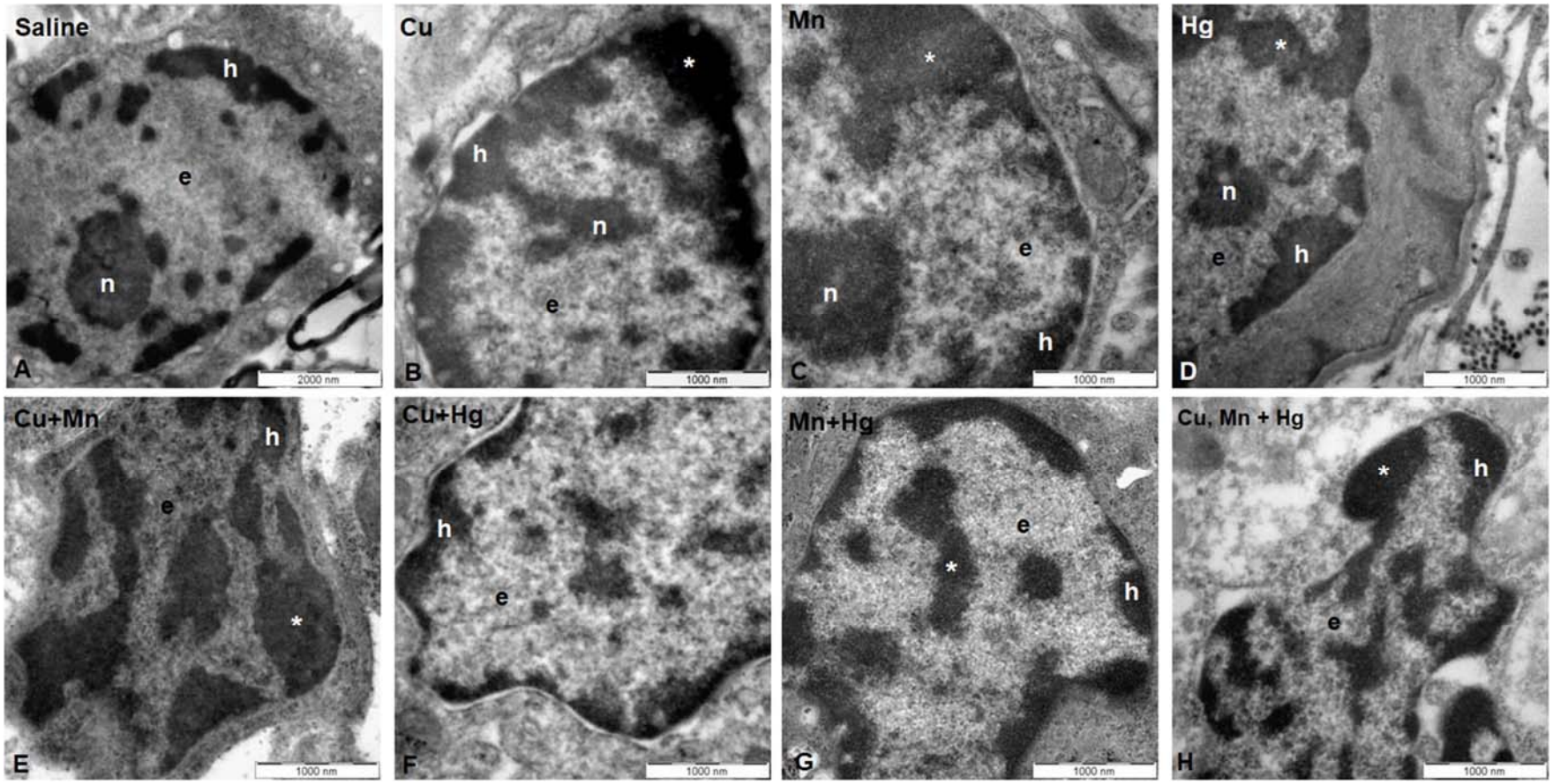
Saline
h
e
n
A
2000 nm
Cu
*
h
n
e
B
1000 nm
Mn
*
e
n
h
C
1000 nm
Hg
*
n
e
h
D
1000 nm
Cu+Mn
h
e
*
E
1000 nm
Cu+Hg
h
e
F
1000 nm
Mn+Hg
e
*
h
G
1000 nm
Cu, Mn + Hg
*
h
e
H
1000 nm

Figure 10

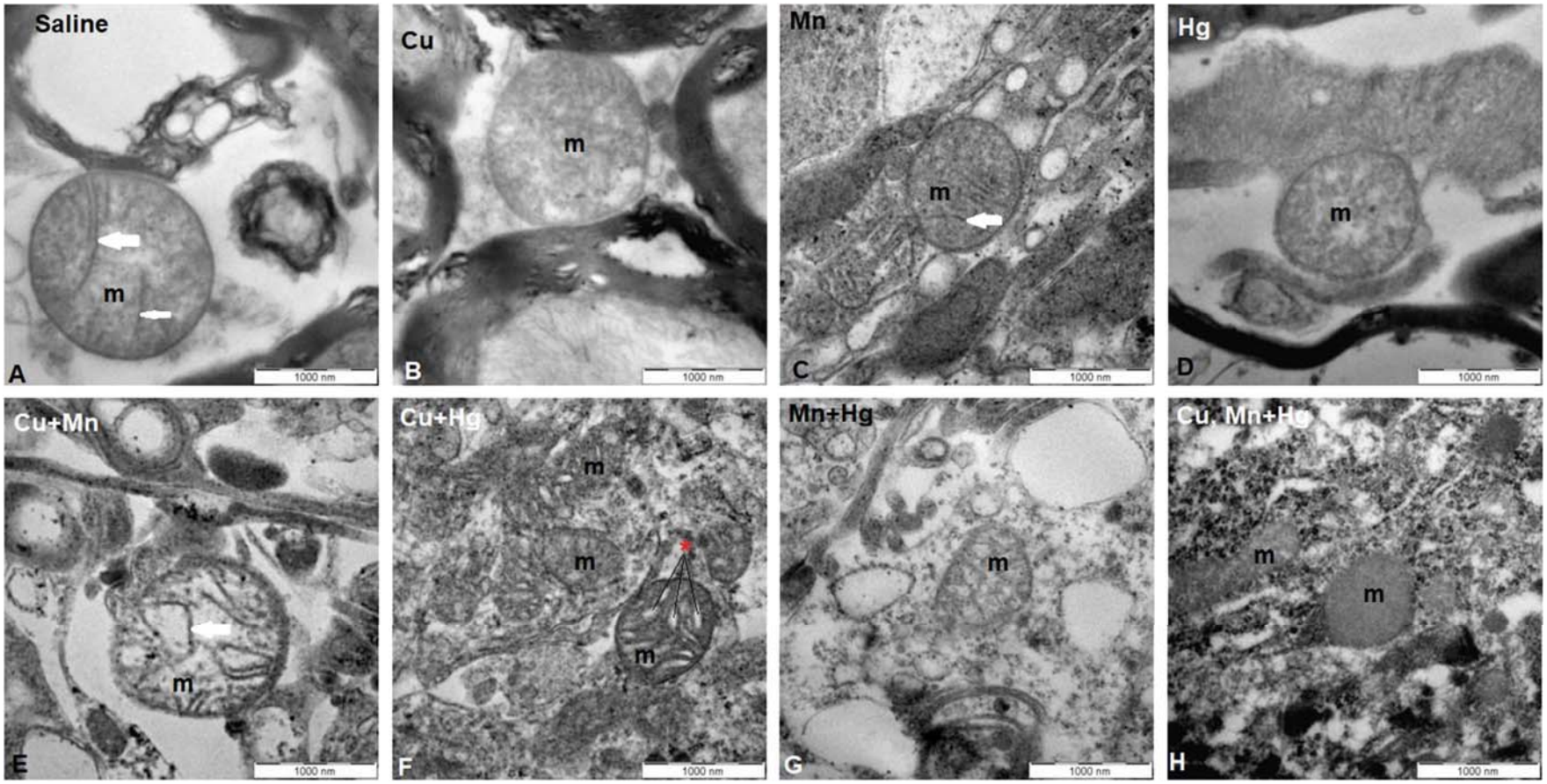
Saline
m
A
1000 nm
Cu
m
B
1000 nm
Mn
m
C
1000 nm
Hg
m
D
1000 nm
Cu+Mn
m
E
1000 nm
Cu+Hg
m
m
m
F
1000 nm
Mn+Hg
m
G
1000 nm
Cu, Mn+Hg
m
m
H
1000 nm